Project Acronym:	FlexiGrid
Project Full Name:	Enabling flexibility for future distribution grids with high penetration of variable renewable generation – FlexiGrid
Grant Agreement:	No 864048
Project Duration:	3.5 years (starting 1 November 2019)

Deliverable D3.2

Report on grid reconfiguration and fault-initiated islanding

Work Package:	WP3-Integrated process for observability, flexibility determination and dispatch
Task:	Grid reconfiguration and fault-initiated islanding
Lead Beneficiary:	TU/e
Due Date:	31/10/2022 (M36) (approved by PO)
Submission Date:	31/10/2022 (M36)
Deliverable Status:	Final
Deliverable Style:	Report
Dissemination Level:	Public
File Name:	Report on grid reconfiguration and fault-initiated islanding

This project has received funding from the European Union's Horizon 2020 research and innovation program under grant agreement No 864048

Table of Contents

Authors ... 3
Reviewers ... 3
Version History ... 3
List of abbreviations ... 4
List of Figures ... 5
List of Tables ... 6
Project overview ... 7
Consortium ... 8
Executive Summary ... 9
1. Introduction ... 10
2. DSO needs for flexibility ... 13
2.1. The operational risk with high DER penetration ... 13
2.2. Needs and requirements for flexibility ... 16
3. Adaptive controller for renewable energy communities ... 17
3.1. Problem formulation ... 17
3.2. Self-adaptive control architecture ... 18
3.3. Simulation and results ... 20
4. Network reconfiguration ... 23
4.1. Problem Formulation ... 23
4.2. A Quasioppositional Chaotic Symbiotic Organisms Search for Network reconfiguration ... 24
4.3. Performance Evaluation ... 25
5. Network risk mitigation based on MPC ... 27
5.1. Voltage contingency ... 27
5.2. Model predictive control for voltage coordination ... 29
5.3. DERs coordination based MPC ... 31
6. Fault-initiated islanding ... 34
7. Conclusions ... 43
8. Appendix A: The physical data of Chalmers campus network ... 44
9. References ... 46

Authors

Surname	First Name	Beneficiary	e-mail address
Tran	Minh-Quan	TU/e	m.q.tran@tue.nl
Tran	Trung	TU/e	t.t.tran@tue.nl

Reviewers

Surname	First Name	Beneficiary	e-mail address
Le Anh	Tuan	Chalmers	tuan.le@chalmers.se
Gazioğlu	İbrahim	OEDAS	ibrahim.gazioglu@oedas.com.tr
Nguyen	Phuong	TU/e	p.nguyen.hong@tue.nl

Version History

Version	Date	Modifications made by
0.01	2022.09.10	First draft
0.02	2022.09.15	Second draft
0.03	2022.10.15	Third draft
0.04	2022.10.31	Final version

List of abbreviations

Abbreviation	Definition
AHO	Andronov-Hopf Oscillator
CPU	Central processing unit
DER	Distributed energy resource
DSO	Distribution system operator
EV	Electric vehicles
HV	High voltage
LTC	Load tap changers
MG	Microgrids
MPC	Model predictive control
MV	Medium voltage
PMU	Phasor measurement unit
PV	Photovoltaic
QC-SOS	Quasi-oppositional Chaotic Symbiotic Organisms Search
VOC	Virtual oscillator control

List of Figures

Figure 1.1: The overview outline of the report structure. 11
Figure 2.1: Production congestion map in the Netherlands on 29/09/2022 [2]. 13
Figure 2.2: Total power of the PV systems in each of Sweden's municipalities [3]. 14
Figure 2.3: A real-time voltage reading at a bus with a high share of solar [4]. 15
Figure 3.1: One-year transformer loading. 18
Figure 3.2: The sequential droop control. 19
Figure 3.3: Self-adaptive control. 19
Figure 3.4: Voltage profile of some houses at community 2 in case of with and without control. 20
Figure 3.5: The transformer loading in case of with and without control. 21
Figure 3.6: Active power of building 07:4.2 in case of with and without control. 22
Figure 3.7: Reactive power of building 07:4.2 in case of with and without control. 22
Figure 4.1: Voltage profile at buses of the modified Chalmers campus network. 26
Figure 5.1: Topology of the tested MV urban power grid. 28
Figure 5.2: Long-term voltage instability. V^{HV}, V^{MV} and LTC are the voltage measured at Bus 0 and 1, and the tap position of the transformer connecting these buses, respectively. 29
Figure 5.3: The voltage V^{HV}, V^{MV} in case of with and without the coordination mechanism. 32
Figure 5.4: The voltage V^{HV}, V^{MV} in case of different prediction horizon. 33
Figure 6.1: Typical hierarchical control structure for DERs. 34
Figure 6.2: VOC-based hierarchical control structures for DERs. 35
Figure 6.3: The estimated impedance. 40
Figure 6.4: PV active and reactive power outputs in case 1. 40
Figure 6.5: PV active and reactive power outputs in case 2. 41
Figure 8.1: One-line diagram of Chalmers campus indicating highlighted renewable energy resources. 44
Figure 8.2: The Chalmers campus network with the communication network among PVs. 45

List of Tables

Table 2.1: Some system disturbances with high DERs integration. 15
Table 2.2: The overview of different solutions for non-contingency and contingency operation. 16
Table 4.1: Performance of the proposed QC-SOS in different case studies. 26
Table 5.1: Performance comparison with different prediction. 32
Table 6.1: Islanding detection solutions. 38
Table 8.1: Line parameter of Chalmers campus network (including some low voltage buses). 45

Project overview

FlexiGrid is an innovation project funded by EU's largest research and innovation program, Horizon 2020.

The project will create an enabling architecture for small and medium Distribution System Operators (DSOs) to unlock flexibility resources. Through a cross-sectoral integration and optimization of resources, especially those arising from coupling between different energy sectors, as well as demand response using charging schemes for electric vehicles (EVs) or storage, DSOs will be able to meet the future capacity shortage with flexibility and updating old systems with smart technology.

In FlexiGrid, organizations from all over Europe cooperate to leverage digital and smart grid technologies at the grid edges. The project will deliver IoT platforms, peer-to-peer and peer-to-pool marketplaces, vehicle-to-grid, power-to-heat, and power-to-gas solutions, as well as innovative business models.

FlexiGrid will equip DSOs with advanced tools to enhance the observability and controllability of distribution networks while demonstrating both pool-based and peer-to-peer market mechanisms. Furthermore, implementing these market mechanisms in the project's demos will be facilitated by a flexible DSO-Customers coordination platform for efficient real-time trading of energy and grid services between market actors.

The overall objectives of FlexiGrid are:

• **To develop an integrated architecture** for flexibility measures and electricity grid services provided by electricity storage, vehicle charging, power-to-heat, demand response, and variable generation to enable additional decarbonization.

• **To define, test, deploy and demonstrate markets and market mechanisms** that incentivize flexibility, in particular for mitigating short-term and long-term congestions or other problems in the distribution network such as voltage issues

• **To drive cooperation** between DSOs, transmission system operators (TSOs), consumers, and generators by defining market interactions, facilitating the integration of wholesale and retail markets, and cross-sector interactions

• **To deploy smart grid technologies** to enable the architecture and markets, bringing actors together to participate as distributed energy sources, driving increased resilience of the electricity grid, increased system security, greater observability, higher automation, and improved control of the grid

• **To enable future technical and commercial innovation** by identifying barriers to innovation, developing pathways to regulatory and policy reform, developing business models, and strategic collaboration.

Consortium


AKADEMISKA HUS

CHALMERS

ENERGO-PRO

EMAX
LIGHT UP THE FUTURE

ENTRA ENERGY

Göteborg Energi

Hes·so
VALAIS
WALLIS

IMCG

inavitas

LUXEMBOURG
INSTITUTE OF SCIENCE
AND TECHNOLOGY
LIST

OEDAŞ
OSMANGAZİ ELEKTRİK DAĞITIM

OIKEN

RI.
SE

SIMAVI

TECHNICAL UNIVERSITY
SOFIA

TU/e
Technische Universiteit
Eindhoven
University of Technology

Executive Summary

This deliverable is a part of WP3's “integrated process for observability, flexibility determination, and dispatch.” The deliverable aims to address potential risks in the network, considering a high penetration of DERs and available grid switch options. Based on the system operation situation, the potential issues are divided into contingency or non-contingency issues. Different methods are developed to solve the detected potential risks.

First, for non-contingency operation issues, such as voltage rise and transformer overloading, an adaptive algorithm is developed in chapter 3. The method is based on local communities with a local controller (i.e., droop controller) to mitigate the voltage rise and reduce the transformer's loading. Thus, the issues are solved by the customers without the need of any action from DSOs. A network reconfiguration method is developed in chapter 4 for DSOs to select an optimal network topology to solve voltage rise and reduce power losses.

Second, in the case of a contingency operation, a model predictive control (MPC) is developed in chapter 5 to improve the voltage profile after a lager disturbance. The available DERs powers and the load tap changer (LTC) are optimal controlled by MPC to support the grid.

Finally, in chapter 6, a fault-initiated islanding algorithm based on Andronov-Hopf Oscillator to autonomous form the microgrid when a fault happens or following the market signals and re-synchronize after the disturbance.

The real data of Chalmers campus network is used to test the above methods. The results confirm the proposed methods' performance in solving the grid's potential issues.

1. Introduction

The integration of distributed energy resources (DER) is the key to achieving zero carbon emissions by 2050 in the energy sector, according to the 26th united nations climate change conference (COP26). On the one hand, it forces the high integration of DERs into the grid, such as solar farms, on/offshore wind farms, heat pumps, and electric vehicles (EV). On the other hand, it faster the phase-out process of existing coal-fired power. It brings different challenges for the DSO to safely operate their grid, such as solving the grid congestion with high shared of DERs, and system stability with low inertia from the synchronous generator.

DSOs need to build a future intelligent distribution system for monitoring and control to tackle the above challenges. Different solutions have been proposed in this WP3 of the H2020 project FlexiGrid. First, the network observability issue is solved using physics-based and data-driven methods. The physics-based method is tested with the Chalmers campus network under task 5.3 of WP5. Then, another task on quantification of flexibility is reported in D3.4, which is based on the guideline in D3.3 about the process design for flexibility procurement and dispatch. Furthermore, an optimal allocation framework for dispatching flexibility is discussed in D3.5. Those tasks solve the grid issues based on demand-side solutions suitable for short-term issues. So, higher impact solutions are needed for larger grid congestion issues or disturbances (i.e., fault or loss of devices).

This report proposes different types of solutions to solve the grid problems in non-contingency and contingency operations. First, depending on the grid's observable states (D3.1), the potential risks are defined as non-contingency (i.e., voltage rise, transformer overloading, or high-power losses) or contingency (i.e., fault with potential voltage instability or system blackout). Then, an adaptive algorithm-based energy community or network reconfiguration is for non-contingency operation. In a case of fault, a model predictive control (MPC) is used to coordinate DERs and load tap changers (LTC) to improve the voltage profile. However, if the system is potentially faced a blackout, fault-initiated islanding is activated to form microgrids (MG) automatically, which secure the continuity of supply for critical parts of the grid. Lastly, the synchronization algorithm can autonomously reconnect the MG with the upstream grid when the fault is cleared.

The deliverable outline is presented below (see Figure 1.1):

- Chapter 2: DSO needs for flexibility will be discussed.

For non-contingency operations, two different solutions will be discussed in Chapters 3 and 4.

- Chapter 3: An adaptive control algorithm to solve voltage rise and transformer overloading issues.
- Chapter 4: A network reconfiguration algorithm to mitigate voltage rise and reduce power loss is developed.

With large disturbances (contingency operation), Chapters 5 and 6 offer two solutions to secure the grid.

- Chapter 5: An advanced MPC algorithm is developed to improve the voltage profile in case of fault.
- Chapter 6: An autonomous fault-initiated islanding algorithm to form MG operation and re-synchronize to the upstream grid is discussed.

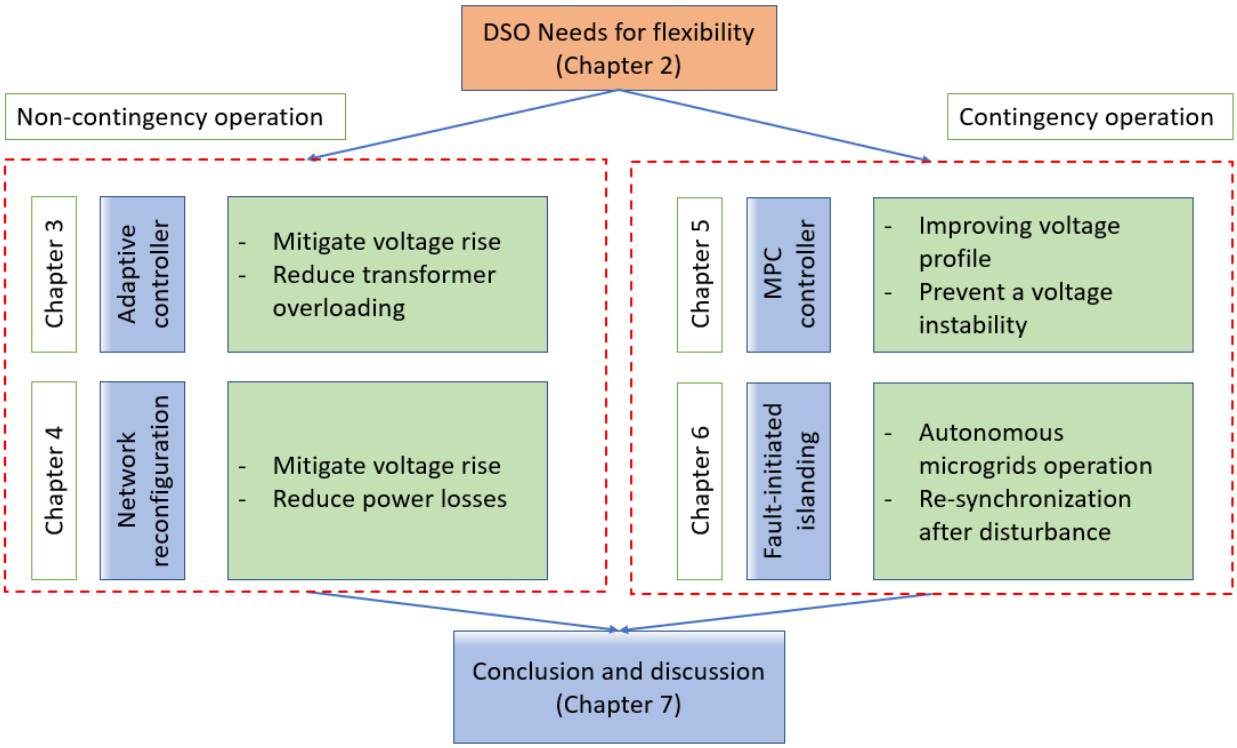

Figure 1.1: The overview outline of the report structure.

The Chalmers campus network is used for the above-proposed methods except for the MPC algorithm since no time-synchronized measurements are available for the Chalmers campus network. The detailed information of Chalmers campus network can be found in Appendix A.

Below is the list the publications which have been publised/accpeted/under review as results from this deliverable:

- Conference papers:

1. M. -Q. Tran, T. T. Tran, P. H. Nguyen, T. T. Mai and L. A. Tuan, "Self-adaptive Controllers for Renewable Energy Communities Based on Transformer Loading Estimation," 2022 IEEE International Conference on Environment and Electrical Engineering and 2022 IEEE Industrial and Commercial Power Systems Europe (EEEIC / I&CPS Europe), 2022, pp. 1-6, doi: 10.1109/EEEIC/ICPSEurope54979.2022.9854677.
   (Open link:
   https://pure.tue.nl/ws/files/204250141/Self_adaptive_Controllers_for_Renewable_Energy_Communities_Based_on_Transformer_Loading_Estimation.pdf)
2. M. -Q. Tran, T. T. Tran, P. H. Nguyen and L. A. Tuan, "Coordination of Load Tap Changer and Distributed Energy Resources to Improve Long-term Voltage Stability," 2022 IEEE 7th International Energy Conference (ENERGYCON), 2022, pp. 1-6, doi: 10.1109/ENERGYCON53164.2022.9830224.
   (Open link: https://pure.tue.nl/ws/portalfiles/portal/198984476/Energycon_2022_Final.pdf)
3. Tran, T., Tran, M-Q., Nguyen, A., Nguyen, P. H., & Tuan, L. A. (Accepted/In press). Virtual Oscillator based Hierarchical Control Strategy for Multi-mode Operation of Microgrids. Paper presented at

12th IEEE PES Innovative Smart Grid Technologies Conference Europe, ISGT Europe 2022, Novi Sad, Serbia.
Open link: https://pure.tue.nl/ws/portalfiles/portal/214369694/ISGT_European_2022_final.pdf)

- Journal papers:

4. M. -Q. Tran, T. T. Tran, P. H. Nguyen, Guus Pemen, 'Sparse Identification for Model Predictive Control to Support Long-term Voltage Stability' accepted in IET Generation, Transmission & Distribution.
5. T. T. Tran, S. K. Gurumurthy, M.-Q. Tran, T.-A. N. Huu, T. Heins, F. Ponci, A. Monti, P. H. Nguyen 'Enhancing Performance of Andronov-Hopf Oscillator based-Grid Forming Converters in Microgrids with Non-invasive Online Impedance Estimation' under review in IEEE Transactions on Smart Grid.

2. DSO needs for flexibility

This report contributes different options for DSO's operation with the integration of DER. Thus, this chapter discusses the operational risk with high DER penetration. Then, the requirements for flexibility options are summarized.

2.1. The operational risk with high DER penetration

Increasing DER into the grid brings opportunities and benefits for the power system and participants. The DERs integration is the key to the current energy transition such as:

- From fossil to renewable energy: in the EEA report [1], the EU has achieved its three 2020 climate and energy targets (i.e., reducing 20% greenhouse gas emission, increasing 20% share of DER, and improving 20% energy efficiency). Furthermore, the new target is a 55% reduction in greenhouse gas emissions by 2030.
- From analog to digital: by using more intelligent grid tonologies and solutions, the end customers are expected to support DSOs in grid management.
- From centralized to decentralized: the local renewable generators and decentralized solutions can help DSO connect with more customers. Furthermore, the customers can be formed as the local community, which can support the grid in case of contingency and non-contingency.

However, DSOs are facing an increase in distribution congestion in their grids. The significant incorporation of high share DERs capacities such as solar, wind farm, and a new type of loads such as heat pumps and EV is created new challenges for DSO. For example, Figure 2.1 shows the Netherlands' production congestion areas due to solar and wind farms. It clearly shows the issue DSO are facing with the high DER penetration in the grids.

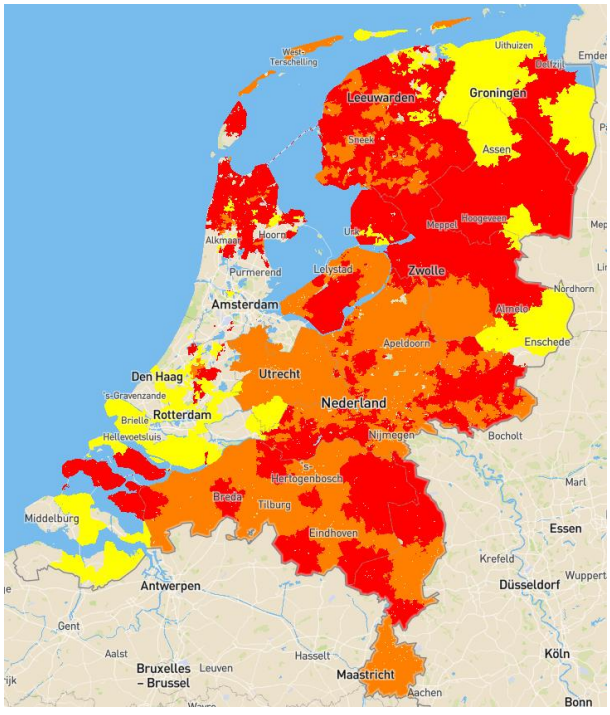

Figure 2.1: Production congestion map in the Netherlands on 29/09/2022 [2].

Similarly in the Netherlands, the grid congestion is reported in Sweden in [3]. Due to the high penetration of DERs as shown in Figure 2.2, it created some power production congestion points in the grid. Those mentioned issues can be defined as two different operation cases non-contingency and contingency, which will be discussed in the following sub-sections.

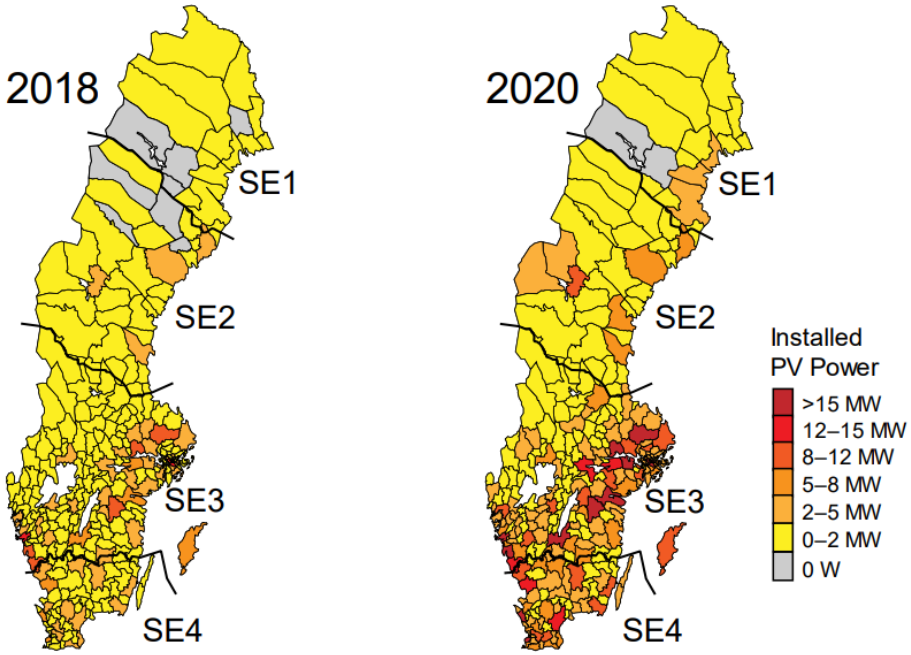

Figure 2.2: Total power of the PV systems in each of Sweden's municipalities [3].

2.1.1. Non-contingency issues

The non-contingency operation is a normal grid operation without any larger disturbance in the grid, such as faults or loss of elements (e.g., generator, transmission lines, transformer, etc.) or unplanned change state of a device (e.g., unplanned opening circuit breaker). However, in this non-contingency operation, the grid still faces many issues with the DERs integration. For example, as mentioned above, the aforementioned production congestion in the Netherlands is one of the most critical issues related to the high solar and wind generation penetration. Besides, the voltage rise, line congestion, or transformer overloading are increasing issues under the DSO's network, as can be seen from Figure 2.3, which clearly shows the overvoltage at a bus with a high share of solar. Furthermore, this voltage fluctuation may lead to increased aging in lines and substation elements.

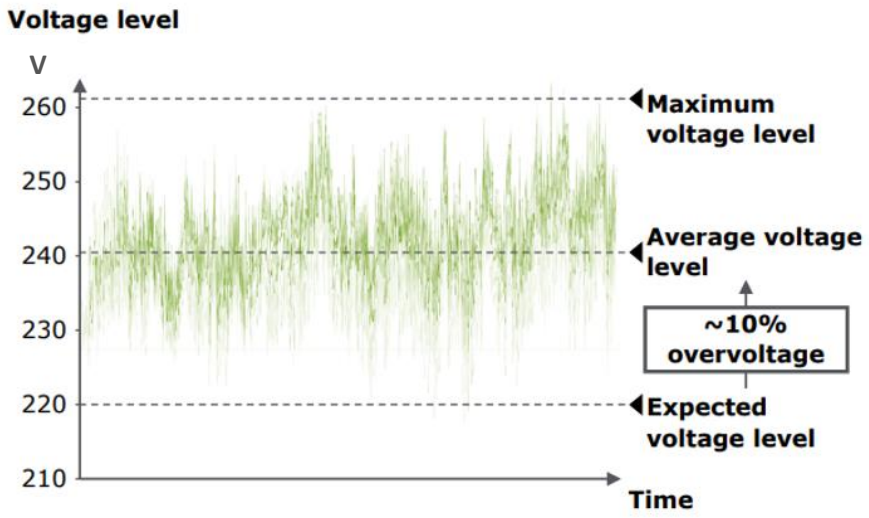

Figure 2.3: A real-time voltage reading at a bus with a high share of solar [4].

2.1.2. Contingency issues

Differ from the non-contingency issues, the direct or indirect negative impacts of DERs on system security are discussed in this chapter. In Table 2.1, different system disturbances involved with DERs recorded worldwide have been summarized. In those disturbances, the leading cause comes from different reasons, such as lighting strikes, faults, or bad weather. The high fault current, over-voltage, or frozen wind farm may lead to the shutdown of DERs, thus pushing the system to a (near) blackout. Therefore, the sensitivity of DERs in such disturbances needs to be considered together with DERs installation.

Table 2.1: Some system disturbances with high DERs integration.

Country/reason and time	Main cause	Sequence of events (related with DERs)	Unexpected result
UK, 2019 [5]	- Three lighting strikes	- Loss of offshore windfarm modules with a total 737 MW	- System backout
Australia, 2016 [6]	- Bad weather, storm	- A larger amount of wind farm was shut down	- System backout
Texas, 2021 [7]	- Winter storm	- Loss of 4GW wind farm due to the frozen of wind turbine	- Large system backout

California, 2022 [8]	-	Phase-to-phase fault on 500 kV line	-	Loss of 765 MW solar and 145 MW of other DERs	-	Large frequency drop

2.2. Needs and requirements for flexibility

As discussed above, the energy transition brings different challenges for system operators in both non-contingency and contingency operations. It requires flexibility options, which can help DSOs optimally manage their system. Different solutions, including demand response, tariff agreements, PV inverter control, network reinforcement, etc., can be used to solve the issues mentioned above. Table 2.2 summarizes different solutions for non-contingency and contingency operations, which define two types of flexibility.

- Demand-side solution: it includes load shifting, tariff agreements, PV curtailment, etc. Usually, the congestion issues such as voltage rise or line/ transformer congestion issues can be solved using the demand-side solution. However, it is only interesting to avoid peak loads and congestion in a short period.
- Grid operation solutions: such as PV inverter control, LTC coordination or network reconfiguration, etc., will have a higher impact on solving grid issues in non-contingency and contingency operations.

Table 2.2: The overview of different solutions for non-contingency and contingency operation.

	Non-contingency	Contingency
Demand-side	- Load shifting - Tariffs agreements - PV curtailment	None
Grid operation	- PV inverter control - LTC control - Network reconfiguration	- PV inverter control - LTC coordination by optimal control - Fault-initiated islanding - Load shedding

This deliverable focus on the grid operation solutions as the flexibility options for DSOs, which will be described in the following chapters.

3. Adaptive controller for renewable energy communities

In this chapter, the transformer overloading and voltage rise issues are solved by the direct control concept. That means the local communities can actively detect the problem and dynamically change their operating conditions to solve the problems. In this case, the DSOs do not need to take any actions until the local communities cannot keep the voltage magnitude and transformer loading in the safe operating range.

Several methods have been proposed to address this problem [9]–[12]. In [9], an overvoltage mitigation method is proposed with droop-based active power curtailment. By computing different set points for the droops, the model offers an equal power curtailment. Further, a power quality management function was developed in [10], which increased network hosting capacity and managed the network voltage rise problem. Authors in [11] proposed a method that regulates the voltage within an acceptable operating range and maximizes the PV generation capacity. The method is based on the local voltage and power measurements, which do not rely on global communication. Recently in [12], adaptive coordination of sequential droop control for PV inverters has been developed to mitigate the voltage rise problem. The method proposed a fair power curtailment while avoiding curtailing a significant PV power by using reactive power absorb. However, it could bring a transformer overloading issue. Thus, in this chapter, the voltage rises, and transformer overloading issues are solve using an adaptive algorithm. The Chalmers campus network is used to test the method.

3.1. Problem formulation

The one-year transformer loading profile of modified Chalmers campus network is presented in Figure 3.1. It can be seen that the transformer loading is very high in the period from mid-April to mid-August. On some days, the loading is over 100%. As a result, the transformer temperature will be increased, corresponding to the overload percentage. Therefore, it will increase failure and reduce the lifetime of the transformer in long-term operation. It can be seen from the figure; the loading percentage is increased at around mid-day. The reason is due to the high-power injection from the PV system. It is noted that the PV system is controlled by local control, named sequential droop control [12]. The Q-V and P-V droop control mitigate the voltage rise problem in radial systems with high PV penetration. The ideal is whenever the voltage is higher than a pre-defined value, and the Q-V droop control is used to calculate the reactive power, which can be absorbed by PV inverters. The voltage difference between sending and receiving buses can be reduced using reactive power, following the equation (3.1).

$$|\Delta V| \approx \frac{(|P_L| - |P_G|)R + (|Q_L| - |Q_G|)X}{|V^*|} \tag{3.1}$$

In that, V^* is the receiving end voltage, P_L/Q_L donate the receiving end bus local power consumption, and P_G/Q_G are the local power generation from PV systems. As a result, the voltage rise problem can be solved while maintaining the large amount of active power injection from household PV. However, in the mid-day, while keeping the active power generation and reactive power absorb from PVs, there is two power flow of active and reactive power through the transformer. As a result, this can cause the transformer to overload. This can reduce the transformer lifetime. In the following sections, we will explain the concept of local communities which can detect the problem and change their power setpoints to solve it automatically.

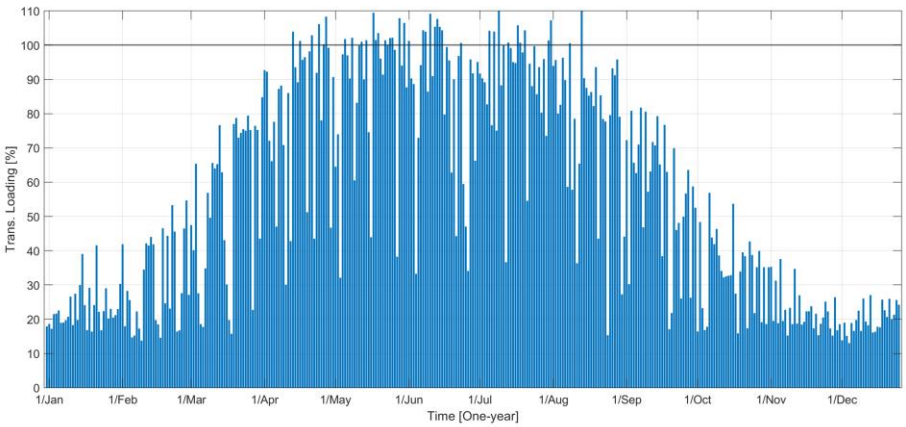

Figure 3.1: One-year transformer loading.

3.2. Self-adaptive control architecture

As described in section 3.1, there is a close relationship between the voltage rise and transformer overloading issues. Therefore, in this section, a self-controlled architecture is developed to solve the voltage rise problem while minimizing the transformer overloading. The term "self-controlled" refers to the active control action from the local energy communities, which can detect the overloading and voltage rise issues then subsequently change their operation setpoints. Each PV is controlled using local droop control, and the active and reactive power setpoints are calculated using the following equations:

For Q calculation (where $\overline{Q}_i$ is the maximum reactive power output, V_i^{tP} is the threshold level of active power curtailment, and V_i^{gQ} is the threshold level for reactive power injection, V_i^{aQ} is the threshold of reactive power absorption):

- If $\underline{V} \leq V_i < V_i^{gQ}$:

$$Q_i^{\text{net}} = \overline{Q}_i \frac{\left(V_i^{gQ} - V_i\right)}{\left(V_i^{gQ} - \underline{V}\right)} \tag{3.2}$$

- If $V_i^{gQ} \leq V_i \leq V_i^{aQ}$

$$Q_i^{\text{net}} = 0 \tag{3.3}$$

- If $V_i^{aQ} < V_i \leq V_i^{tP}$

$$Q_i^{\text{net}} = -\overline{Q}_i \frac{\left(V_i - V_i^{aQ}\right)}{\left(V_i^{tP} - V_i^{aQ}\right)} \tag{3.4}$$

- If $V_i^{tP} < V_i \leq \overline{V}$

$$Q_i^{\text{net}} = -\overline{Q}_i \tag{3.5}$$

For P calculation (where P_i^{MPP} is the maximum power point):

- If $\underline{V} < V_i \leq V_i^{tP}$:

$$P_i^{\text{net}} = P_i^{\text{MPP}} \tag{3.6}$$

- If $V_i^{tP} < V_i < \overline{V}$:

$$P_i^{\text{net}} = P_i^{\text{MPP}} - P_i^{\text{MPP}} \frac{\left(V_i - V_i^{tP}\right)}{\left(\overline{V} - V_i^{tP}\right)} \tag{3.7}$$

- If $V_i \geq \overline{V}$:

$$P_i^{\text{net}} = 0 \tag{3.8}$$

The set of equations from (3.2) to (3.8) can be summarized in Figure 3.2. If the PV voltage reaches the reactive power threshold V_i^{aQ} (at the point (1)), the PV will start absorbing reactive power to reduce the voltage in the grid. However, if the voltage still increases and go over the V_i^{tP} (at point (2), which is the threshold level of active power curtailment), the PV injection from PV will be decreased.

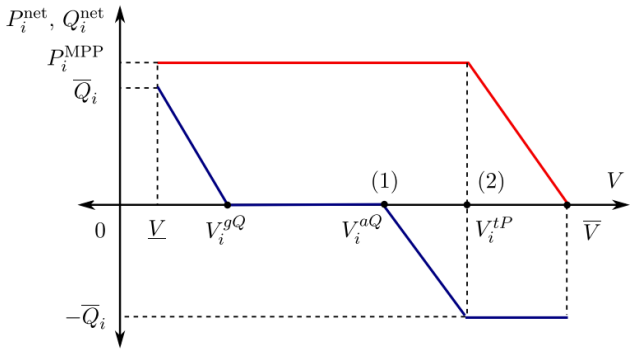

Figure 3.2: The sequential droop control.

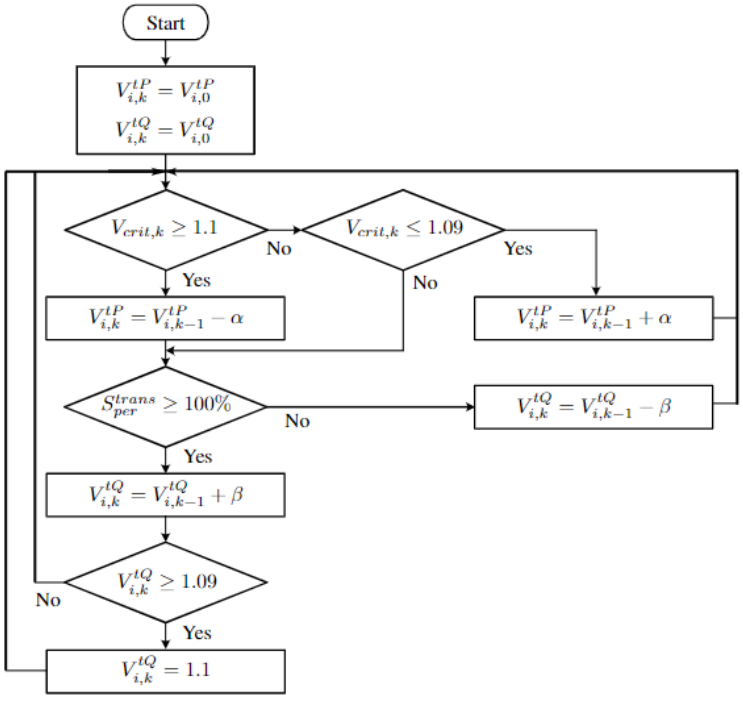

Figure 3.3: Self-adaptive control.

A self-adaptive control is developed on the higher control layer to monitor the transformer loading and mitigate the voltage rise issues. Figure 3.3 shows the control diagram of the proposed control. The control is based on the voltage magnitude of the critical bus in each community (the house near the end of feeders) and the estimated transformer loading status to adaptive increase or decreases the setpoint of active curtailment and reactive power absorption. The active power injection needs to be curtailed whenever the voltage exceeds the operation limit of 1.1 pu. Together with the voltage control, the transformer loading is monitored, the overloading limit is set at 95%. If the loading is higher than the limit, then the threshold of Q absorption is increased, which means the PV will reduce the reactive power absorption.

3.3. Simulation and results

The concept of self-adaptive control is applied in the modified Chalmers campus network (check the Appendix A for more detail). The distribution network is built in MATLAB/Simulink, and the control is developed using S-Function. Figure 3.4 shows the voltage profile at the bus 07:4.2 (with a higher voltage). We compare the result in two cases - with and without self-adaptive control (local control is used in both cases). Since there is no voltage rise issue in the Chalmers campus network. So, for the purpose of testing the method, we set the maximum voltage is 1.4 pu as the maximum allowed voltage. As can be seen that, there is a over voltage period around 9am to 4pm as the time having more PV injection power. Then, in the case of having adaptive control, the voltage is controlled below 1.4 pu. However, there is a yellow are area, where the voltage is higher the set point of 1.4. The reason is the reaction of the controller for the transformer overloading areas.

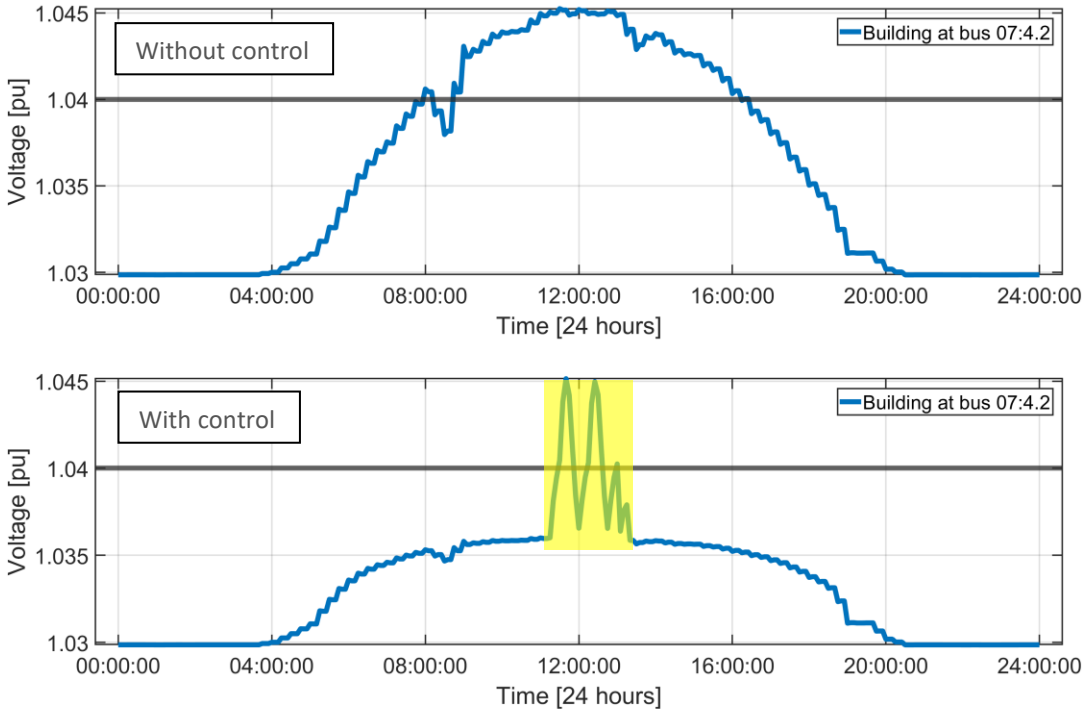

Figure 3.4: Voltage profile of some houses at community 2 in case of with and without control.

The transformer loading in the case of with and without control is shown in Figure 3.5. During the mid-day, the loading percentage increases due to the active power injection and reactive power absorption. As can be seen from the Figure, the overloaded transformer period (over 95%) is effectively reduced by using the self-adaptive control. Figure 3.6 and Figure 3.7 show the absolute value of active power injection and reactive power absorption of building 07:4.2. As shown in Figure 3.7, the reactive absorption increases following active power injection when the loading percentage is still under the threshold. In the case of transformer overloaded, the threshold for reactive power absorption is increased (the point (1) in Figure 3.2 is moved to the right) to reduce the absorbed reactive power. As a result, the reactive power absorption decreases to zero to prevent the transformer from overloading. However, the transformer is still overloaded, meaning that the active power injection needs to be reduced. Figure 3.6 shows that the active power injection is not equal to the maximum power point corresponding to the overloaded transformer period. At this time, the active power injection is increased up to the maximum power point. This simulation results show the proposed control method can regulate the power output of PVs system to effectively control the voltage rise and transformer overloading issues.

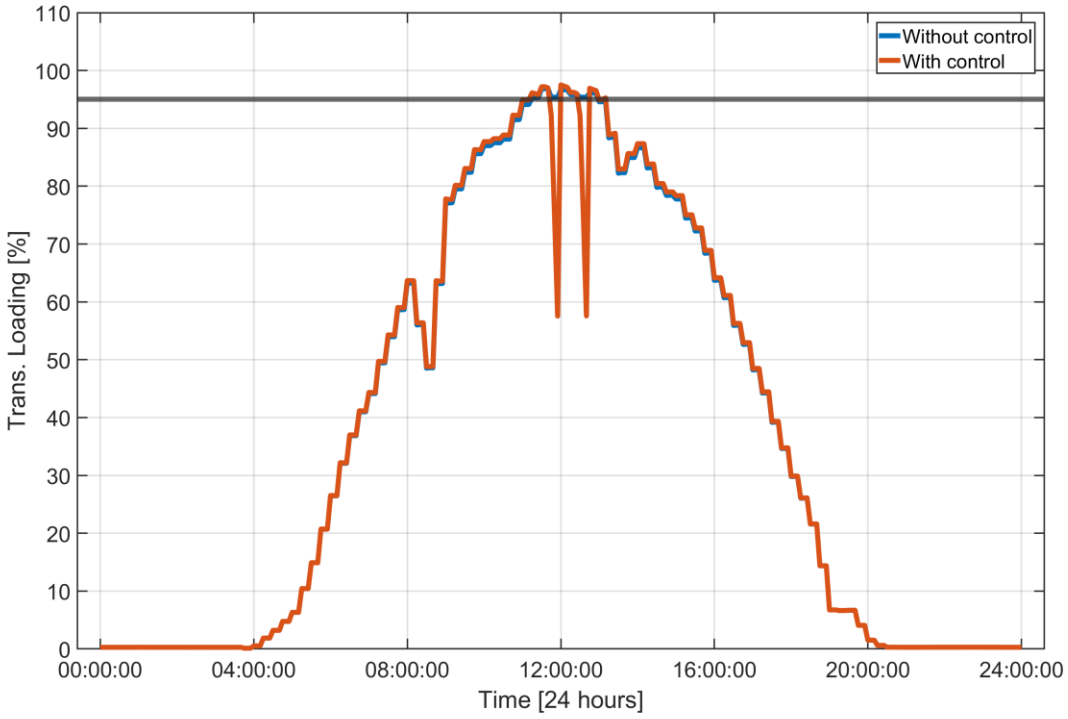

Figure 3.5: The transformer loading in case of with and without control.

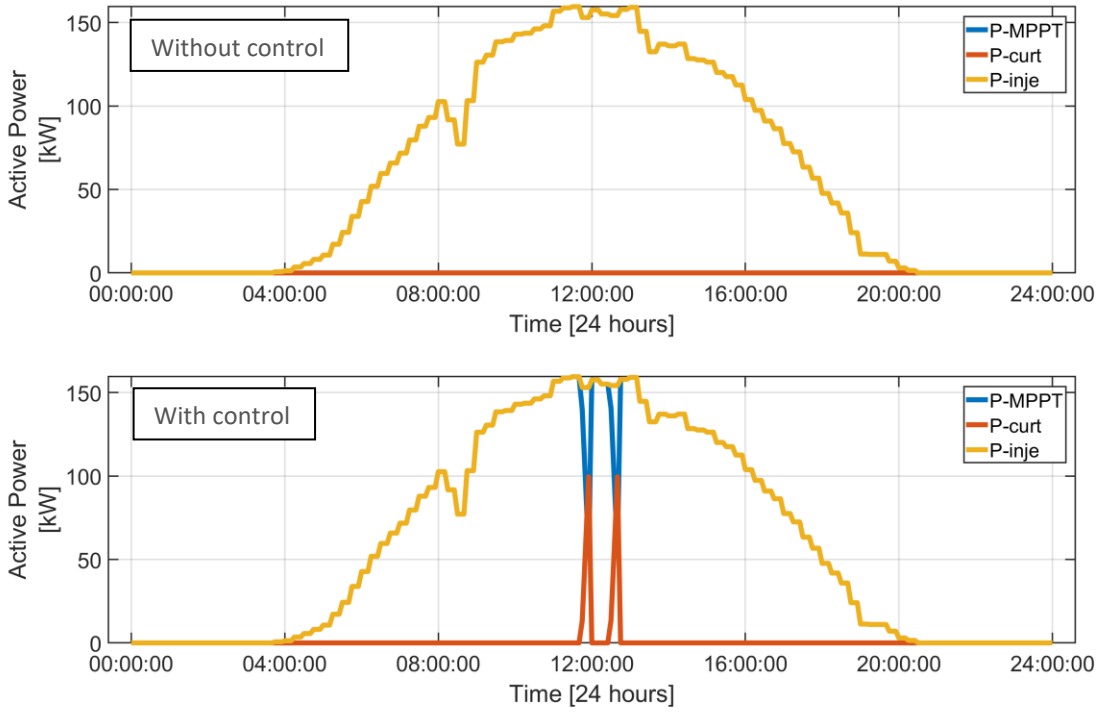

Figure 3.6: Active power of building 07:4.2 in case of with and without control.

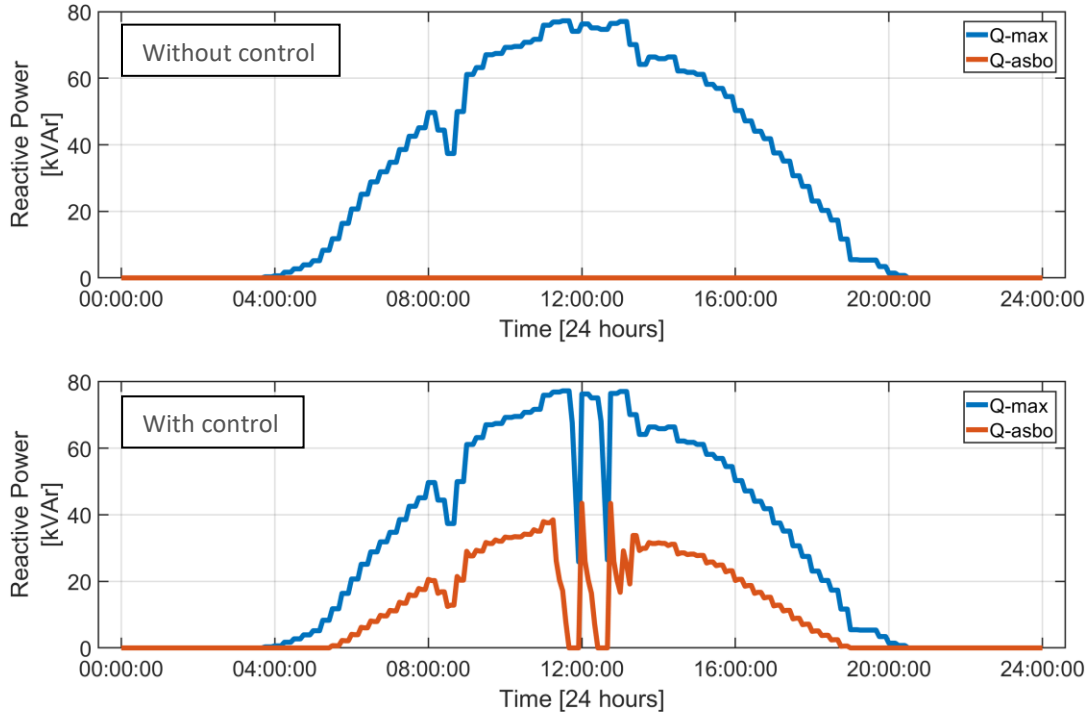

Figure 3.7: Reactive power of building 07:4.2 in case of with and without control.

4. Network reconfiguration

In this chapter, the network configuration is used to solve the non-contingency operation in the distribution grid. Increasing research attention has been paid to improve the resilience and reliability of future power systems to mitigate the adverse effects of DERs. Utilizing network reconfiguration, both static (for planning phase) and dynamic (for operational phase) is a promising approach to achieve this goal [15]. The below sub-sections present a development of control algorithms to reconfigure (static) and separate (dynamic) a certain network area according to existing conditions and market signals to increase flexibility and reliability in operating the distribution grid, given the high penetration of DERs and automated gears. Network reconfiguration is an effective method to minimize the power loss in distribution networks, improve the voltage profile and system reliability. This chapter presents a metaheuristic method based on the Quasi-oppositional Chaotic Symbiotic Organisms Search (QC-SOS) algorithm. The proposed algorithm aims to optimize the network configuration subject to the minimum active power loss and enhanced voltage profile at each bus in distribution networks.

4.1. Problem Formulation

The main goal of the proposed method is to minimize the active power loss (P_{loss}) in the distribution network, while the voltage profiles at buses are kept within predefined limits and other operating constraints are satisfied. The overall objective function is as follow:

$$min \sum_{i=0}^{N_b} P_{Loss} = min \sum_{i=0}^{N_b} R_b I_b^2 \tag{4.1}$$

Subject to:

a. Voltage profile constraint:

$$0.95\ pu \leq V_i \leq 1.1\ pu \tag{4.2}$$

b. Power balance constraint:

$$P_G + \sum_{i=1}^{N_{DER}} P_{DER,i} = \sum_{j=0}^{N_L} P_{L,j} + \sum_{k=0}^{N_b} P_{Loss,k} \tag{4.3}$$

$$Q_G + \sum_{i=1}^{N_{DER}} Q_{DER,i} = \sum_{j=0}^{N_L} Q_{L,j} + \sum_{k=0}^{N_b} Q_{Loss,k} \tag{4.4}$$

c. Thermal limit:

$$|I_b| \leq |I_{max,b}| \tag{4.5}$$

d. DER power limit:

$$P_{DERmin,i} \leq P_{DER,i} \leq P_{DERmax,i} \tag{4.6}$$

e. Radial configuration constraint:

The radial topology must be maintained after reconfiguration. This constraint can be achieved if the following condition is satisfied:

$$|det(A)| = 1 \tag{4.7}$$

where A is the matrix representing the connection of branches and buses in the distribution network. $|A_{ij}| = 1$ if there is a connection between i and j, otherwise $|A_{ij}| = 0$.

4.2. A Quasioppositional Chaotic Symbiotic Organisms Search for Network reconfiguration

The SOS method is developed based on the concept of cohabitation behavior of unlike organisms in natural ecosystem, i.e., the relationship between two distinct species. Three common symbiotic relationships, namely mutualism, commensalism and parasitism, are used in the proposed QC-SOS method. Starting from a random population of an ecosystem, the search process updates the population following the aforementioned phases, until the termination criteria and the optimal solution are achieved. The implementation of the proposed QC-SOS to reduce total power loss and improve voltage profiles at all buses in the distribution network is explained in the following sub-sections.

4.2.1. Ecosystem Initialization

In this step, number of organisms (eco size), initial ecosystem and termination criteria are determined. Each organism O_i denotes a solution vector which consists of switches that will be opened.

$$O_i = [SW_1 \quad \dots \quad SW_{N_{SW}}] \tag{4.8}$$

where N_{SW} is the total number of opened switches as an optimal solution of the QC-SOC method.

Each organism is randomly generated based on its predefined boundaries, as follow:

$$SW_i = round\left[SW_{min,i} + rand(0,1) \times \left(SW_{max,i} - SW_{min,i}\right)\right] \tag{4.9}$$

To improve the obtained solution quality and convergence speed of the method, the Quasiopposition-based Learning (QOL) is embedded into the SOS algorithm. QOL is performed when SOS generates a random initial population of the ecosystem, or when a new population is calculated. The opposite point of each organism O_i^o is calculated as follow:

$$O_i^O = O_{min,i} + O_{max,i} - O_i \tag{4.10}$$

Then, a quasiopposite point O_i^{qO} is given as follow:

$$O_i^{qO} = rand\left(\frac{O_{min,i} + O_{max,i}}{2}, O_i^O\right) \tag{4.11}$$

From the set $[O_i, O_i^{qO}]$, the fitness values for organisms are calculated, and *N* best organisms are chosen as initial populations, as follow:

$$B_F = OF + K_V \sum_{i=1}^{N_B} \left(V_i - V_i^{lim}\right)^2 + K_T \sum_{i=1}^{N_L} \left(I_k - I_k^{lim}\right)^2 \tag{4.12}$$

where, K_V and K_T are the penalty coefficients for voltage at branches and thermal current of loads, respectively.

The radial configuration of the distribution network is checked for the chosen initial organism. Then the main loop is implemented for the first iteration.

4.2.2. Mutualism Phase

The mutual relationship vector between the j^{th} random organism and i^{th} organism in the population is determined as follow:

$$MV = \frac{O_i^{qO} + O_j^{qO}}{2} \tag{4.13}$$

Then new organisms are created as follow:

$$O_i^{qO\_new} = O_i^{qO} + rand(0,1) \times (O_{best} - MV \times BF_1) \tag{4.14}$$

$$O_j^{qO\_new} = O_j^{qO} + rand(0,1) \times (O_{best} - MV \times BF_2) \tag{4.15}$$

where BF1 and BF2 are random number chosen as 1 or 2, O_{best} is the best organism in the population.

The fitness value of the new organisms is calculated, and new organisms are updated if their new fitness values are smaller than the old ones. Otherwise, the set of organisms is kept the same.

4.2.3. Commensalism Phase

In this phase, an organism i^{th} is randomly chosen from the population and is updated with the assist of organism j^{th} based on commensalism interaction. A new organism is generated as follow:

$$O_i^{qO\_new} = O_i^{qO} + rand(-1,1) \times \left(O_{best} - O_j^{qO}\right) \tag{4.16}$$

$O_i^{qO\_new}$ is used to replace the old organism if its fitness value is smaller than that of the old one, similar to the previous phase.

4.2.4. Parasitism Phase

In this phase, one random organism i^{th} is chosen as a parasite to get benefit from a random host organism j^{th}. $O_i^{qO\_new}$ is duplicated to create a so-called parasite vector (PV) O_{PV}^{qO}. This vector is used to update the vector $O_j^{qO\_new}$ as follow:

$$O_j^{qO_new} = \begin{cases} O_{PV}^{qO}, & if\ f(O_{PV}^{qO}) < f\left(O_j^{qO_new}\right) \\ O_j^{qO_new}, & if\ otherwise \end{cases} \tag{4.17}$$

The whole process is repeated for the whole ecosystem size. When the termination criteria is achieved, the process is done and optimal solution will be extracted.

4.3. Performance Evaluation

The performance of the proposed QC-SOS is tested on the modified Chalmers campus network, which presented in Figure 8.1, in the Appendix A. The original Chalmers campus network has 23 buses and 8 PV systems installed mostly on the roof of the buildings. To validate the developed method, it is assumed that all branches connecting buses are able to switch on or off to reconfigure the network. In addition, three branches (S23, S24 and S25) are added to find the optimum solution for the tested network to have minimum active power loss and improve voltage profile at all buses. For ease of implementation, 8 PV systems are only the available DERs on the network.

At the beginning, the tested network is operated at original configuration with S1 – S22 are closed and S23 – S25 opened (base case). The PV systems are operated at the MPP to supply the local loads, and the

surplus power is fed back to the utility grid. The total active power loss of the base case is 3.5% of active power. The size of the ecosystem is set as 50, and the maximum iteration is 300. The QC-SOS method obtained the opened switches: S13, S21, and S24, where the active power loss of the network is reduced by 1.8% compared with the base case. Table 4.1 presents the obtained active power loss when varying the ecosystem's size and the number of the iteration. The calculation time is significantly reduced with smaller values of these parameters. It is also noted that since the topology of the tested network is simple in size and complexity, changing the parameters of QC-SOS does not affect the optimal results. However, in a more complex and larger network, there is always a trade-off between the computational burden and the quality of the optimal solutions. Choosing the right size of the ecosystem and maximum iteration is significant then. Figure 4.1 shows the voltage of buses of the tested system. It is obvious that by finding the optimal network configuration, the voltage profiles are also improved when compared to the base case.

Table 4.1: Performance of the proposed QC-SOS in different case studies.

Case study	Ecosize	Maxiter	Ploss (% of Pload)	CPU time (s)
1	5	5	2.9%	0.32
2	5	300	2.1%	15
3	20	300	1.8%	60
4	50	100	1.8%	50
5	50	300	1.8%	247
6	Normal network		3.5%	

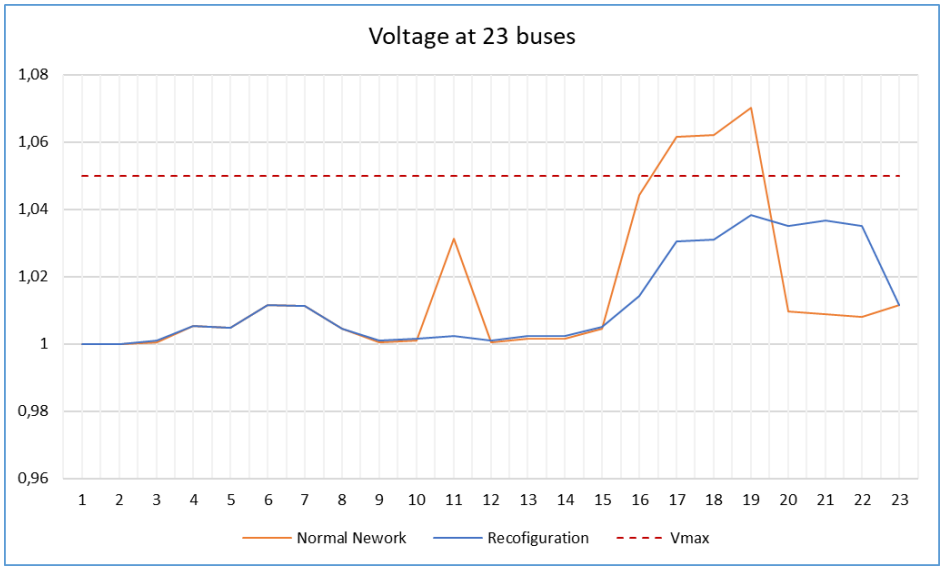

Figure 4.1: Voltage profile at buses of the modified Chalmers campus network.

5. Network risk mitigation based on MPC

Due to a lack of power supply to the (passive) distribution network after emergencies, an issue of long-term voltage instability might occur [16]. One the one hand, the presence of distributed energy resources (DER), e.g., solar PV, wind, or storage, can be considered to resolve this issue. On the other hand, the coordination of DERs with the existing grid controller, i.e., load tap changer (LTC) is essential to secure the operation between transmission and distribution networks. This has been highlighted also by ENTSO, ISGAN, NERC [17]–[19].

The coordination between DERs and LTC has been investigated in [20]–[23] to address instability issue at the primary side of the high-voltage/medium-voltage (HV/MV) transformer. The main cause of this issue is the presence of voltage-dependent load which creates an adverse effect on the primary side of the transformer while LTC reduces the tap set point to keep the voltage at the secondary side of the transformer within the bound. In [20], a distributed model predictive control (MPC) is developed to keep the voltage of multi-area within the acceptable bounds. However, the nonlinear dynamic of DERs are neglected which might cause possible conflicts between the coordination strategy and DER's local constraints. Reference [21] presented a centralized MPC to regulate the distribution network voltage with the high penetration of DERs. The MPC model is designed with a constant prediction horizon which is unnecessary and time-consuming in case of small voltage deviation. In [22], three control strategies are developed to control DERs and LTC to increase the power transfer into an affected area, thus increasing the voltage stability margin. Further, the voltage instability mechanism in the transmission system due to control actions in the distribution system is explained in [23]. Then, the authors proposed a synchronization of LTC actions and DERs to support long-term voltage stability. However, the sequential control of DERs and LTC leads to unnecessary LTC control actions which reduces the lifespan of the transformer, as well as increases the recovering time of voltage.

The nonlinear dynamic of DERs needs to be taken into account when their capability in voltage control is explored [24]–[26]. In [24], an adaptive proportional-integral controller is developed for multiple inverters to regulate DERs's terminal voltages. It shows that the voltage correction of the other DERs may result in over-voltage at another DER's terminal bus, leading to a need of system-wide coordination. In [25], authors investigated the challenging of DERs integration in low voltage (LV) network, the risks related to disconnecting DERs in LV networks when voltage rise occur and active power curtailment approaches are proposed to mitigate the problem of voltage rise. Further, adaptive coordination of sequential droop for PV is developed in [26] to solve the voltage rise problem while being able to reduce the amount of power curtailment. However, the coordination of DERs together with other grid controllers such as LTC during stressed operation conditions (e.g., after a large disturbance) is still a challenge.

This paper aims to investigate the capability of DERs to support long-term voltage stability. First, we reformulate the stability problem, considering essential elements such as LTC, and voltage dependent load. Second, we investigate a possible coordination scheme to ensure the support of DERs and LTC in emergencies. Lastly, a simulation is performed in a modified CIGRE MV benchmark network to show the benefit of adequately coordinating between the grid operator and DERs

5.1. Voltage contingency

To better understand the voltage instability problem that can occur in urban power grid during emergency cases, a European MV distribution network benchmark is used, as shown in Figure 5.1. The MV urban

power grid is assumed to connect to the utility grid via two parallel transmission lines. A simulation is performed in which a three-phase fault is considered at one of the two parallel transmission lines between external bus and Bus 0. This transmission line trips at time t = 0 to isolate the fault. After a short-term period with dynamics assumed to be stable, the system enters a long-term period where voltage stability is of concern. In general, this period involves slow-acting equipment such as LTC, Over Excitation Limiter (OXL) of a synchronous generator and controlled loads.

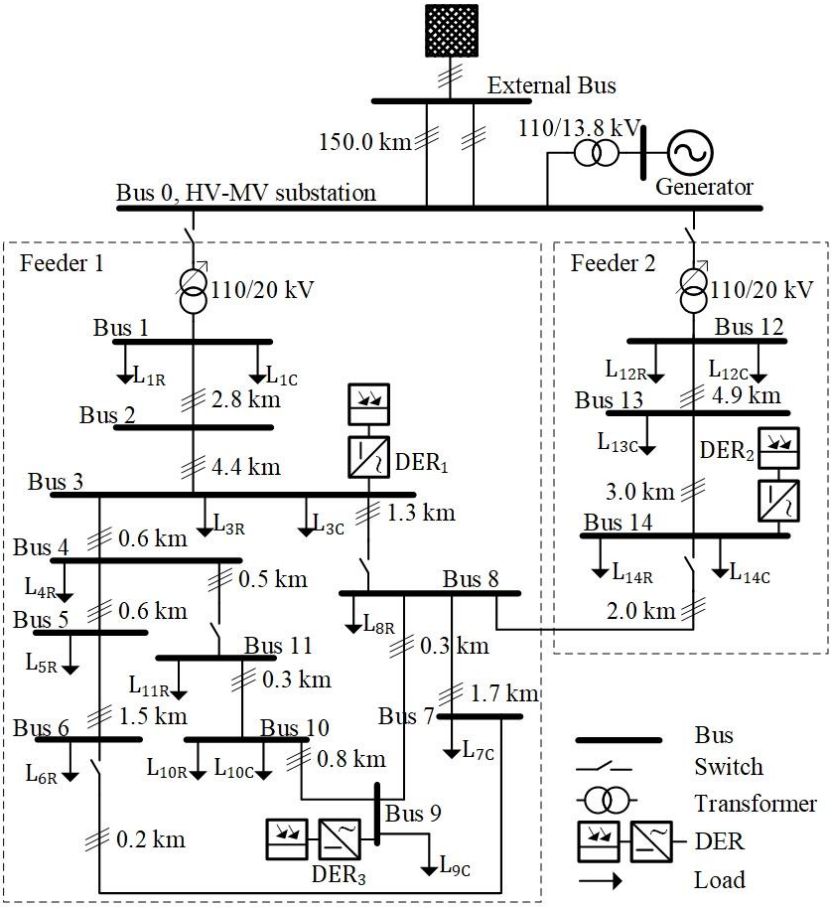

Figure 5.1: Topology of the tested MV urban power grid.

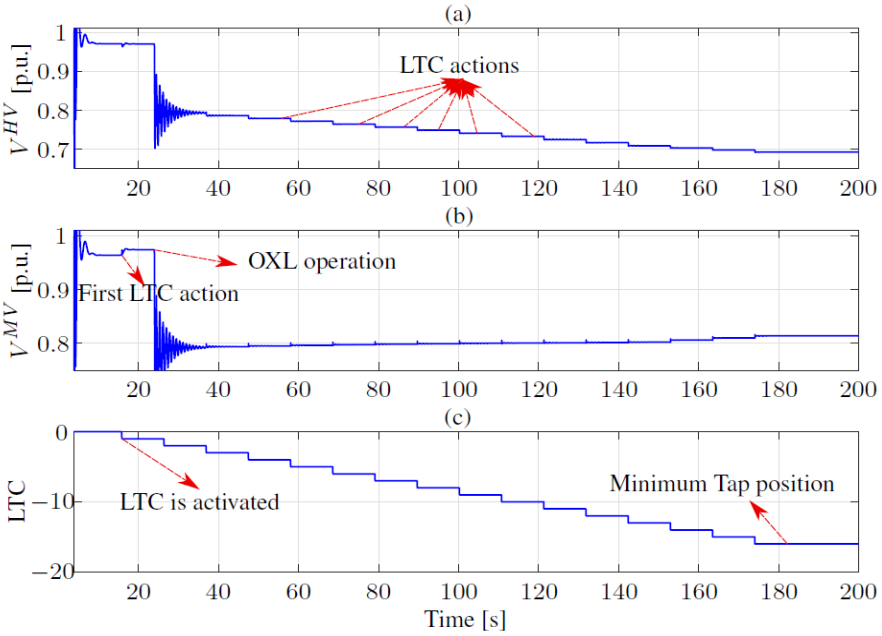

Figure 5.2: Long-term voltage instability. V^{HV}, V^{MV} and LTC are the voltage measured at Bus 0 and 1, and the tap position of the transformer connecting these buses, respectively.

As seen from Figure 5.2, a short transient period occurs following the tripping of the transmission line. After that, the voltage at two sides of the transformer V^{HV}, V^{MV} are stable at 0.973 pu and 0.928 pu, respectively. As a result, the LTC controller changes the tap position to increase V^{MV}, aiming to bring this voltage back to nominal value, i.e., 1 pu. It should be noted that the LTC action is activated every fixed period of 15 seconds and the first activation is at t = 15 s.

At t = 24 s, the voltages V^{HV}, V^{MV} are dropped further to 0.815 pu and 0.824 pu, as the OXL circuit is activated to protect the generator winding from the fault. Consequently, the LTC controller continues to change the tap position of the transformer to increase the voltage V^{MV}. The increase of V^{MV} along with the LTC actions results in the increase of active and reactive power consumption from voltage-dependent loads, causing the increase in the total load consumption in the urban power grid. However, the limited power transfer capacity is reached due to the tripping of a transmission line. Consequently, the voltage V^{HV} is continuously decreased below the acceptable operating range. This may activate the low voltage protection system which can lead to cascading tripping of other transmission lines and even causing the whole system to be collapse.

5.2. Model predictive control for voltage coordination

In recent years, the coordination between DERs and LTC for voltage stability support has received increasing attention from researcher. In [27], a voltage constrained centralized management was developed based on a physics-based model in form of sensitive matrix. A centralized Model Predictive Control (MPC) is developed in [21] to regulate the distribution network voltage using the steady-state voltage sensitivity analysis, which is extracted from an offline power flow calculation. In [20] the concept of distributed MPC was developed for long-term voltage coordination in multi-area power system. This method assumes that voltage of all buses can be observed locally via the phasor measurement units (PMUs). Then a distributed MPC is implemented using spare communication network.

Beside the physics-based methods, data-driven methods are also promising solutions to improve voltage monitoring and control. In [28], an artificial neural network (ANN) is applied to identify the voltage sensitivity matrix which then used for voltage prediction in the centralized MPC model. Recently, in [29], the authors use ANN to build a control knowledge between system dynamics and optimal control actions, thus supporting the controller to find optimal solutions faster.

This section presents a coordination method combining centralized MPC method and a voltage prediction model to support long-term voltage stability. The voltage evolution is predicted online based on system Jacobian matrix. Then, it is used as the predictor for the MPC model, where the optimal control action for LTC and DERs are determined. The primary goal of the method is to use available power supplies from DERs, especially ES units to effectively restore the voltage at the grid edges back to the pre-fault conditions with a minimum number of LTC control actions.

MPC is an advanced control method that use a discrete-time model of a system to predict the future behavior of the desired control variables and compute a set of future control actions by optimizing an objective function with predefined constraints. The MPC can solve a single or multiple objectives together with discrete and continuous control variables. Here, the overall objective is to identify and call for available resources (LTC action and DER generation) to support restoring voltage after emergency conditions, expressed as follows:

$$min \sum_{i=0}^{N_c-1} \|\Delta V(k+i)\|^2_{R_v} + \|\Delta V^T(k+i)\|^2_{R_T} \tag{5.1}$$

Subject to

$$\begin{cases} u^{min} \le u(k+i) \le u^{max} \\ \Delta u^{min} \le \Delta u(k+i) \le \Delta u^{max} \\ 0.9\ pu \le V_k^{MV} \le 1.1\ pu \end{cases} \tag{5.2}$$

For $i = 0, 1, \ldots N_c - 1$. where $\Delta u(k) = \left[\Delta P_k^{DER}, \Delta Q_k^{DER}, \Delta V_k^T\right]$is the change of the control variables at time step k compares to step k – 1. Rv and RT are weight matrices for voltage regulation and LTC actions used to determine the priority of the control variables.

The voltage prediction model for MPC is expressed as follows:

$$V_{k+1}^{HV} = V_k^{HV} + \frac{\partial V_k^{HV}}{\partial P_k^{DER_j}} \Delta P_k^{DER_j} + \frac{\partial V_k^{HV}}{\partial Q_k^{DER_j}} \Delta Q_k^{DER_j} + \frac{\partial V_k^{HV}}{\partial V_k^T} \Delta V_k^T \tag{5.3}$$

where V_k^{HV} is the voltage measurement at the time step k. $\partial V_k^{HV}/\partial V_k^T$ is the voltage sensitivity matrix with respect to an LTC position. $\partial V_k^{HV}/\partial P_k^{DER_j}$and $\partial V_k^{HV}/\partial Q_k^{DER_j}$ are the voltage sensitivity matrices corresponding to the change of the reactive and active power, respectively. These terms can be obtained using the inverse of the system Jacobian matrix J, as follows:

$$\begin{bmatrix} \Delta\delta_2 \\ \vdots \\ \Delta\delta_n \\ \Delta V_2 \\ \vdots \\ \Delta V_n \end{bmatrix} = J^{-1} \begin{bmatrix} \Delta P_2 \\ \vdots \\ \Delta P_n \\ \Delta Q_2 \\ \vdots \\ \Delta Q_n \end{bmatrix} \quad (5.4)$$

where $\Delta\delta_i$ and ΔV_i are the absolute change in voltage angle and voltage magnitude at bus i which corresponding to the change in active (ΔP) and reactive ($\Delta\delta_2$) power.

5.3. DERs coordination based MPC

In this section, a simulation has been implemented using MATLAB/Simulink to evaluate the effectiveness of the coordination mechanism. The numerical results were obtained on a ThinkPad Laptop with an Intel Core (TM) i7-8750 central processing unit (CPU), 2.20 GHz processing speed and 16 GB random access memory (RAM).

The modified MV European benchmark distribution system is used as the tested system with the topology shown in Figure 12.6 and parameters are explained in [30]. The main system parameters are presented as follows:

- The MV distribution system is supplied by an external grid via two parallel transmission lines, represented by a 110 kV/50 Hz three-phase voltage source, with a short-circuit power of 500 MVA and R/X ratio of 0.1.
- The system nominal voltage: 3-phase, 20 kV (Line to Line), 50 Hz.
- The transformer with an LTC controller is installed between Bus 0 and Bus 1, which is designed to keep the voltage at Bus 1 within a range from 0.985 pu to 1.015 pu.
- A synchronous generator with OXL contributing to the long-term voltage issue is installed at the HV/MV substation.

The coordination mechanism is used to support the voltage dynamics by optimizing the LTC action and mobilizing the available power supply from DERs. The MPC algorithm is installed at the Application Control Layer of the hierarchical controller. The performance of the method is validated by comparing the voltage stability in the case of with and without the coordination.

Figure 5.3 presents a time sequence of the control actions. After a short stable transient period, the voltage V^{HV}, V^{MV} enter a long-term voltage period. The recorded pre-fault primary voltage is $V_0^{HV} = 0.996\ pu$. As the voltage V^{HV} is dropped in contingency case, the coordination mechanism is activated to bring it back to the pre-fault value.

The simulation results show that, V^{HV} is smoothly brought back to the pre-fault value while keeping V^{MV} in a predefined limit (i.e., [0.9, 1.1] pu). In this case, the prediction horizon of MPC is 2 steps ahead. As can be seen from Figure 5.4, in the period from t = 22 s to t = 80 s the voltage is slightly increased while the LTC is kept unchanged. This is the advantage of multi-objective-based control. In this period, the power from DERs is still available. Thus, the MPC keeps the LTC position unchanged and use only power from DERs to support the voltage. In the next period t = 80 s to t = 140 s, the powers from DERs reaches their limits. Thus, the coordination mechanism must use the support from the LTC operation to keep increasing V^{HV} back close to the nominal value.

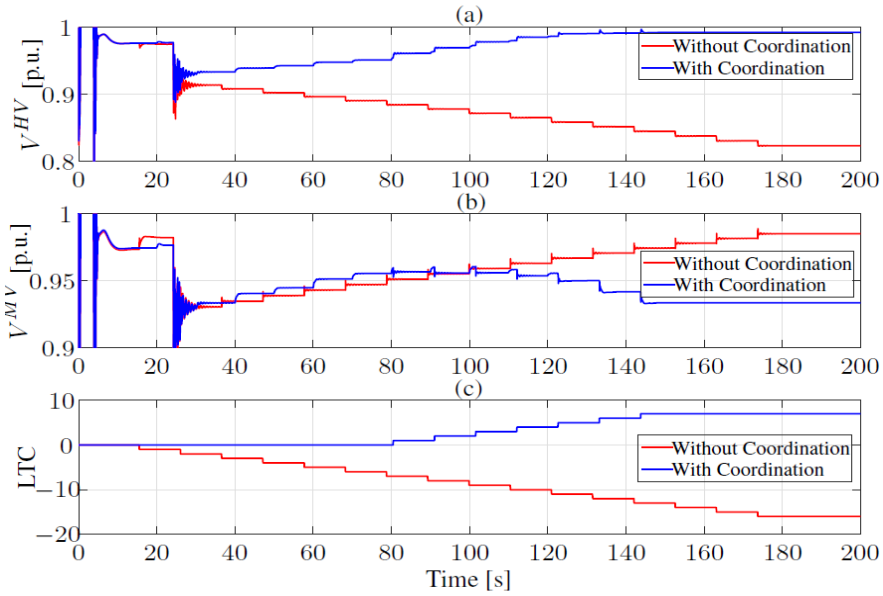

Figure 5.3: The voltage V^{HV}, V^{MV} in case of with and without the coordination mechanism.

Figure 5.4 compares the performance of the coordination mechanism with different prediction horizon of the MPC controller. As shown, with N = 2, the MPC controller starts to change the LTC position at around t = 80 s, while the time with N = 5 and N = 8 is around t = 90 s and t = 160 s, respectively. As the result, V^{HV} is recovered faster when using least number of the prediction horizon with the cost of more LTC actions. On the contrary, the computational burden is increased with a longer prediction horizon. This trade-off can be reduced by using adaptive prediction horizon for MPC controller, which is out of the scope of this section.

Table 5.1: Performance comparison with different prediction.

Prediction Step	LTC actions	Simulation time (mins)
2	7	**16.27**
5	7	**25.51**
8	**5**	**38.22**

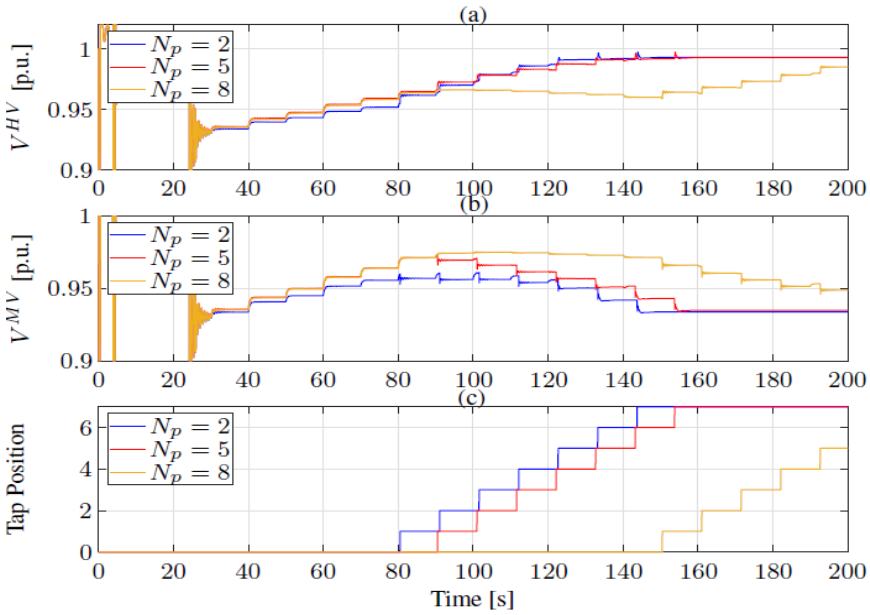

Figure 5.4: The voltage V^{HV}, V^{MV} in case of different prediction horizon.

In this chapter, model predictive control has been proposed for the purpose of voltage support. The controller was designed to coordinate the LTC of the transformer and DERs in an active distribution network to commonly support voltage at the primary side of the transformer. The simulation results in the CIGRE benchmark for the European medium voltage distribution network verify that our method is able to bring the voltage back to the pre-fault value. Different case studies were analyzed showing the high performance of the proposed MPC controller. In the case of using a longer prediction horizon for the MPC, it can faster bring the voltage back to the reference value while minimizing the number of LTC actions.

6. Fault-initiated islanding

Different from the chapter 4, which used the network reconfiguration to solve the grid in non-contingency operation. This chapter introduces a control strategy for power electronic interfaces of DERs in a specific area of the distribution system. The proposed control strategy provides a dynamic reconfiguration functionality in term of fault-initiated islanding to increase the system reliability and maintain the continuity of supply during and after the faults.

Different control methods have been described in the existing literature to provide a complex, multiple target coordination for diverse DERs in distribution grid, and hierarchical control structure is among the most effective solutions. Typical hierarchical control structures for DERs are presented in Figure 6.1 which consists of multiple control layers with proper time-scale separation property. The overall control objective is to enable DERs to operate in both grid-connected and off-grid, i.e., islanded, mode, as well as seamless transition between two modes. The lowest control layer (Converter Control Layer) can use multi-stage controller combining of current, voltage and droop control loops [31]. The key control function of this layer is to maintain system stability during both steady-state and transient periods. The Application Control layer is the main control mechanism for voltage and frequency regulation, allowing DERs to share the load powers in off-grid mode and follow the power setpoints in grid-connected mode. Advanced control technologies applied to this layer enable additional functions and auxiliary services such as voltage, current distortion compensation, disturbance rejection, and synchronization. The existing typical decentralized control method for this layer is the droop control method. Alternatively, single-stage controllers such as Virtual Oscillator Control (VOC) [32], or Self-Synchronized Synchronverters [32] approach, can be used to ensure functionalities of both control layers. It means the complexity of the overall control structure is reduced, making it easier to implement in real devices.

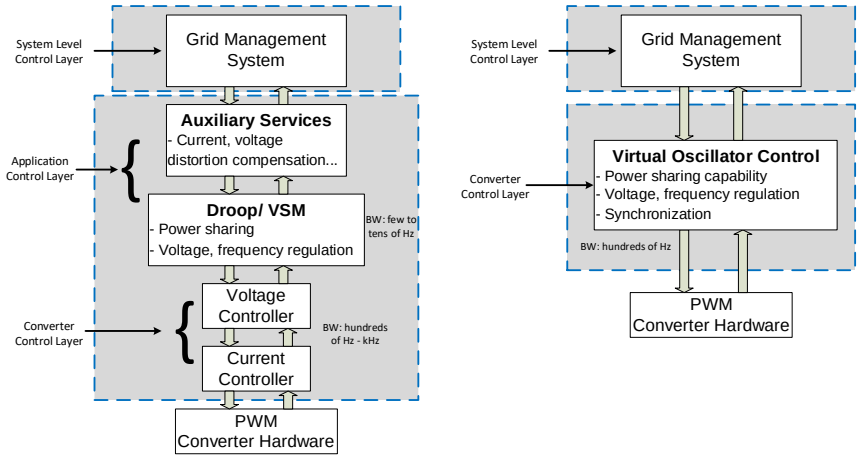

Figure 6.1: Typical hierarchical control structure for DERs.

The proposed strategy allows DERs to have the following functionalities:

- When faults are happened and an area of the distribution system is disconnected from the main utility grid, the controllers are able to detect the disconnection and switch to off-grid (islanded) control mode to continuously supply local (critical) loads by using local generations.

- When faults are cleared, the isolated area is able to smoothly reconnect to the main utility grid and the controllers of DERs can switch to grid-connected mode to generate power following commands from higher control layer (e.g., market, ancillary service signals, etc.).

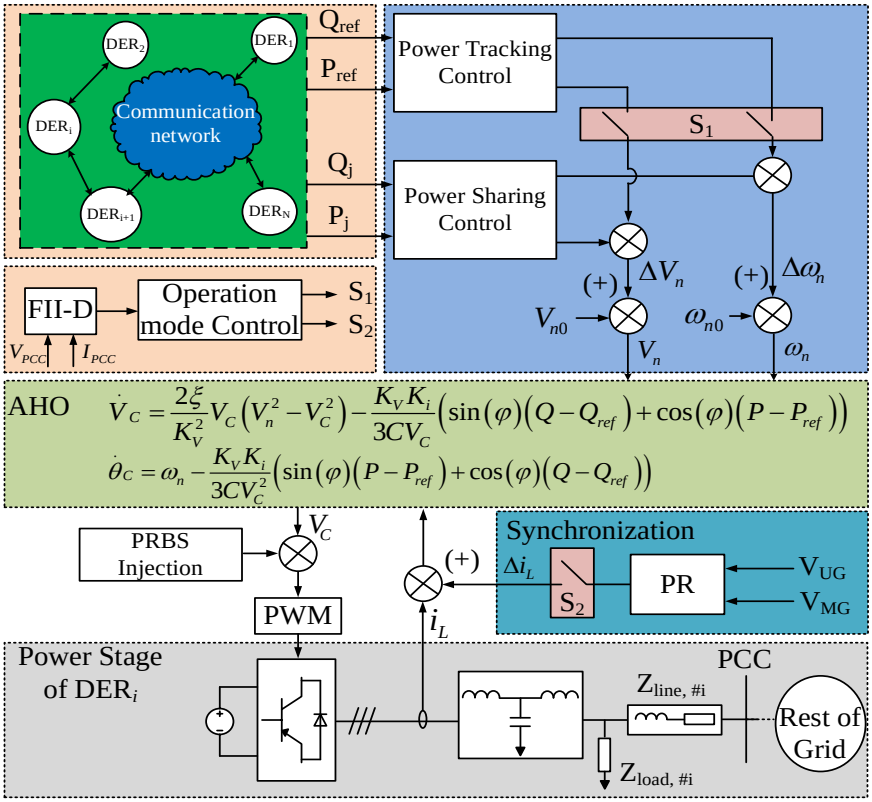

Figure 6.2: VOC-based hierarchical control structures for DERs.

Figure 6.2 presents the proposed control strategy in detail. In this structure, DERs communicate with others through a communication network, either centralized or distributed based on different applications. The Andronov-Hopf Oscillator (AHO) is used for Converter Control Layer. The dynamics of AHO is realized by two differential equations as shown in block AHO in Figure 6.2. The Power Tracking Control and Power Sharing Control adjust the internal parameters of AHO (i.e., V_n and ω_n) to regulate the active (P_i) and reactive power (Q_i) outputs of DER$_i$ following the commands from upper control levels (P_{ref} and Q_{ref}). The Fault-Initiated Islanding Detection (FII-D) changes the status of switch S_1 and S_2 to change the operation mode of DER. The detailed explanation of each control block is given in the following sections.

6.1.1. Andronov-Hopf Oscillator

The AHO is utilized on the primary control layer to obtain precise power-sharing among DER units, stable voltage and frequency in an islanded mode without requirement of communication links. It also features the functionality to track active and reactive power setpoints from system operators in grid-connected mode. The dynamics of AHO is represented by the following model, considering the magnitude (V_C) and phase angle (θ_C) of AHO voltage output as state variables:

$$\dot{V}_C = \frac{2\xi}{K_V^2} V_C (V_n^2 - V_C^2) - \frac{K_V K_i}{3CV_C}\left(\sin\varphi\,(Q - Q_{ref}) + \cos\varphi\,(P - P_{ref})\right) \quad (6.1)$$

$$\dot{\theta}_C = \omega_n - \frac{K_V K_i}{3CV_C^2}\left(\sin\varphi\left(P - P_{ref}\right) + \cos\varphi\left(Q - Q_{ref}\right)\right) \quad (6.2)$$

where ω_n and V_n are the nominal system frequency and voltage, ξ governs the speed of convergence to steady-state. K_i and K_V are the scaling factors that couple AHO input and output to physical electrical feedback signals, respectively.

Similar to other VOCs, AHO uses filter inductor current (i_L) as an input to generate the PWM modulation signal (V_C) required to drive the VSC. In order to improve the performance of the conventional AHO, two internal parameters of AHO, namely nominal voltage V_n and nominal frequency ω_n, are adaptively adjusted to fulfill desired control objectives based on the outputs of secondary control layer, as follows:

$$V_n = V_{n0} + \Delta V_n \quad (6.3)$$

$$\omega_n = \omega_{n0} + \Delta\omega_n \quad (6.4)$$

where V_{n0} and ω_{n0} are the initial values, ΔV_n and $\Delta\omega_n$ are the adaptive term of V_n and ω_n, respectively.

In grid-connected operation, AHO controls the power outputs of DER following the setpoints from upper control level. Whereas, in islanded operation, the power setpoints are set equal to 0, i.e., $P_{ref} = Q_{ref} = 0$. By doing this, DERs share the load power in proportion to their power rating, achieved by appropriately setting the scaling factors.

6.1.2. Power Sharing Control of DERs

In the off-grid mode, the control objective is to provide continuous, reliable, and stable power supply from DERs and/or ES units for the critical loads and areas, e.g., balancing between generation and load by using power-sharing control method.

The accurate power sharing mechanism of AHO is achieved by properly setting the scaling factors in proportion to the VSC power ratings with the assumption that the equivalent impedance seen from the output of VSCs has the same order of magnitude as the power sharing ratio. However, it is a great challenge to achieve correctly that equivalent impedance because of the lack of network information, the complexity of network topology, load position and the differences of feeder impedances. The Power Sharing Control, taking advantages of consensus control technique, is proposed to enhance the power sharing accuracy among DERs in complex networks. The communication network must fulfill the necessary and sufficient conditions of graph theory, explicitly presented in [33]. In the proposed method, each DER iteratively exchanges and updates the information of their neighbors (active P_j and reactive Q_j power outputs) to recalculate the global setpoints for DERS $[P_{ave}, Q_{ave}]$ as follows:

$$\Delta P_{ave} = \frac{1}{N}\sum_i^N P_i \quad (6.5)$$

$$Q_{ave} = \frac{1}{N}\sum_i^N Q_j \quad (6.6)$$

where N is the total number of dispatchable units, P_i and Q_i is the active and reactive power output of each DER unit, respectively.

The mismatches between DER power outputs and the required setpoints are compensated by using a Proportional-Integral (PI) controller of the form in

$$\Delta V_n = \left(K_P^V + \frac{K_I^V}{s}\right)(P_i - P_{ave}) \quad (6.7)$$

$$\Delta \omega_n = \left(K_P^\omega + \frac{K_I^\omega}{s}\right)(Q_i - Q_{ave}) \quad (6.8)$$

where K_P^V, K_I^V, K_P^ω and K_I^ω are the controller coefficients. ΔV_n and $\Delta \omega_n$ are internal control variables of VOC associated with active and reactive power control, respectively.

6.1.3. Power Tracking Control of DERs

In grid-connected mode, network operators are responsible to distribute the active (P_{ref}) and reactive (Q_{ref}) power setpoints from an upper-level dispatch center to dispatchable sources, according to optimal economic operation, or request for ancillary services from network operators. The control objective of Power Tracking Control located in the *Application Control Layer* is to compensate for the mismatch between DER power outputs and the required setpoints, simply using a Proportional-Integral (PI) controller which is similar to the previous section:

$$\Delta V_n = \left(K_P^V + \frac{K_I^V}{s}\right)\left(P_i - P_{ref\_i}\right) \quad (6.9)$$

$$\Delta \omega_n = \left(K_P^\omega + \frac{K_I^\omega}{s}\right)\left(Q_i - Q_{ref\_i}\right) \quad (6.10)$$

6.1.4. Synchronization Framework

When the fault is resolved and the power supply from the utility grid is available again, the off-grid area can be reconnected again with a proper synchronization mechanism. To enable a seamless reconnection of the isolated area and prevent severe consequences, at the moment of closing the circuit breaker at the point of common coupling (PCC), the voltages at two sides of circuit breaker have to stay within a strict limit for a required time period [34]. The basic idea of the synchronization framework presented in Figure 6.2 is used to adjust power setpoints of all dispatchable units in a distributed cooperative manner so that the voltage mismatch between two sides of circuit breaker is closely reduced to 0 using Proportional-Resonant (PR) controller, given as follows:

$$G_{PR}(s) = K_P + K_I \frac{\omega_c s}{s^2 + 2\omega_c s + \omega_n^2} \quad (6.11)$$

where K_P and K_I are the proportional and resonant coefficients, respectively; ω_c and ω_n are the cutoff and system nominal frequency, respectively.

6.1.5. Fault-Initiated Islanding Detection

The fault-initiated Islanding (FII) is a method to detect faults and disconnect a part of distribution system from the main utility grid and allow it to operate as an autonomous islanded grid. In this occasion, the disconnected area is supplied by local generations such as PV and energy storage units, until the fault is cleared, and this part is reconnected to the rest of the grid. In recent years, FII has received increasing attention as it allows network operator to reduce the risk of supply losses to critical loads, areas without huge investment in network components [35].

The FII detection can be generally categorized into communication and local methods, as shown in Table 6.1. The communication-based methods rely on high-speed two-way communication to detect the abnormal operation of remoted assets, then provides status checking information as an input for fault detection algorithm installed in a central controller. These methods can be applied for every type of dispatchable generations with reliable detection performance. The main disadvantages of these methods

are the availability and high cost of communication system, and low flexibility to topology changes [36]. The local methods can be further divided into active (i.e., introducing disturbance to the grid and observe the response) and passive methods (i.e., observing locally the variation in voltage, frequency, or power to make the correct tripping decision).

Figure 6.2 presents an active method based on the estimation of the impedance change is used to detect the disconnection of the main utility grid. The method consists of two steps. First, it injects a wideband Pseudo Random Binary Sequence (PRBS) to the control input of a dispatchable source and then a wideband non-parametric impedance at the PCC (Z_{PCC}) in frequency domain $Z_{PCC}(\omega) = V_{PCC}(\omega)/I_{PCC}(\omega)$ is estimated from the voltage (V_{PCC}) and current measurement (I_{PCC}), based on the Discrete Fourier Transform (DFT). Second, the parametric impedance estimation is obtained based on a complex curve fitting technique with a first order polynomial function, as follows:

$$Z_{PCC}^{par}(s) = R_{PCC} + L_{PCC}s \tag{6.12}$$

The magnitude of PRBS disturbance must be chosen carefully, considering the trade-off between the estimation performance and the quality of the power supply. It is known that the impedance of the utility grid is smaller than the impedance of the local load. Then, the estimated impedance output seen from a dispatchable source will be much smaller in grid-connected mode than in off-grid mode. Therefore, by continuously estimating the impedance, it is allowed the detection of islanding situation. In this case, a notification signal is sent to other dispatchable sources via communication network to change the operation mode accordingly.

FII can be done through a sequence of actions, including

- The FII detects fault,
- The circuit breaker is opened to isolate the affected area
- The FII sends the control signals to changes the status of switch S_1 and S_2 to change the operation mode of DERs.

Table 6.1: Islanding detection solutions.

Category	Technology	Characteristics
Centralized	Communication based [37], [38]	- Require high-speed communication system - High detection performance with low non-detection zone - Vulnerable to network topology changes
Local	Active methods [39], [40]	- Intentionally inject a disturbance to analyses the behavior of affected systems - Reduced size of non-detection zone - Trade-off between detection performance and quality of power

Passive methods [41], [42]	- Directly obtain system variables (voltage, frequency, power) to detect islanding - Have no impact on power quality, fast detection speed - Large non-detection zone
Hybrid methods [43]	- Employs both active and passive detection techniques - Improve performance of individual methods - Effective in complex systems

6.1.6. Performance Evaluation

This section validates the operation and performance of the discussed hierarchical control structure in supporting dynamic network reconfiguration by providing fault-initiated islanding functionality. The parameters of the control schemes are presented in detail. Selected waveforms from several case studies are reported for discussion.

6.1.6.1. System under test

The Chalmers network in the Appendix A is used again for this chapter, this network is simulated in MATLAB/Simulink. For simplicity of evaluating the proposed FII method, only 8 PV panels are used as DERs. The communication network among PVs is virtually simulation, as shown in Figure 8.2. Each PV exchanges active and reactive power output information to their neighbors through a spare communication network (noted with red dotted line). The circuit breaker CB is used to connect or disconnect the test system from the main utility grid. The controller of the main circuit breaker communicates with only PV_1 for distributed synchronization purpose. An individual PV system is interfaced with the test system via an LCL filter and a DC-AC inverter and is controlled by the hierarchical control strategy. The system parameters are briefly described as follows:

- The parameters of AHO are chosen following the design process presented in [44]
- Power Tracking Control: (K_P^V, K_I^V) 0.0025, 0.0002
- Synchronization controller: (K_P, K_I, ω_c) 0.0098, 3, 0.63.

6.1.6.2. Transition from grid-connected to off-grid mode

This scenario aims at demonstrating the performance of the FII detection method to isolate the tested system from the main distribution system. The tested system is assumed to operate in grid-connected mode. Under the control of hierarchical controller, all PVs generate power based on the active and reactive power setpoints from the dispatch center (see Figure 12.4 (a) and (b) at t = 0 - 4 (s)).

The impedance estimation algorithm is activated at *t = 2 (s)* and is run continuously every 1 second. Figure... shows how the PRBS signal disturbs the output of AHO. The whole estimation process takes around 0.4 seconds to finish. In grid-connected mode, the estimated magnitude of the impedance seen from the PCC of PV_1 is 0.025 Ω (see Fig. 3a). At *t = 4 (s)*, a fault is assumed to happen that causes the CB to open to disconnect the tested network from the main distribution system. From *t = 4 -4.4 (s)*, as the FII Detection has not yet detected the change in the impedance, a large transient of active and reactive power happens. If this situation remains for a long time period, system instability or severe consequences may happen. At *t = 4.4 (s)*, the FII Detection sees a significant change in estimated impedance and sends a

control signal S1 to change the operation mode from power-tracking to power-sharing mode. After a short transient period, the isolated network reaches an equilibrium point where all PVs share the load powers proportional to their rated powers.

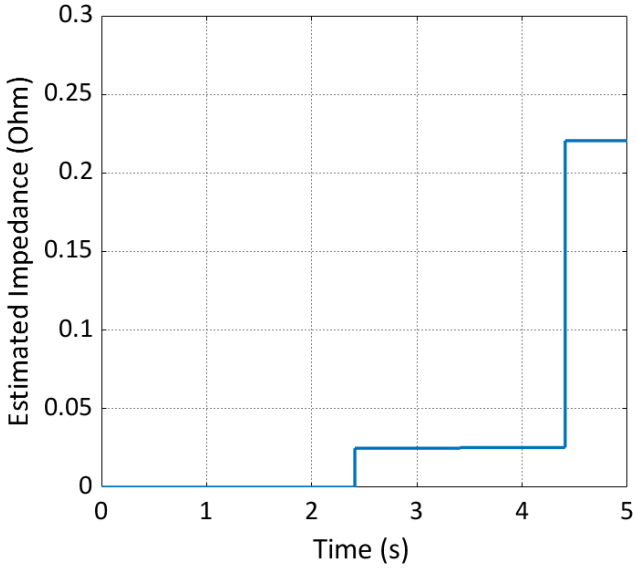

Figure 6.3: The estimated impedance.

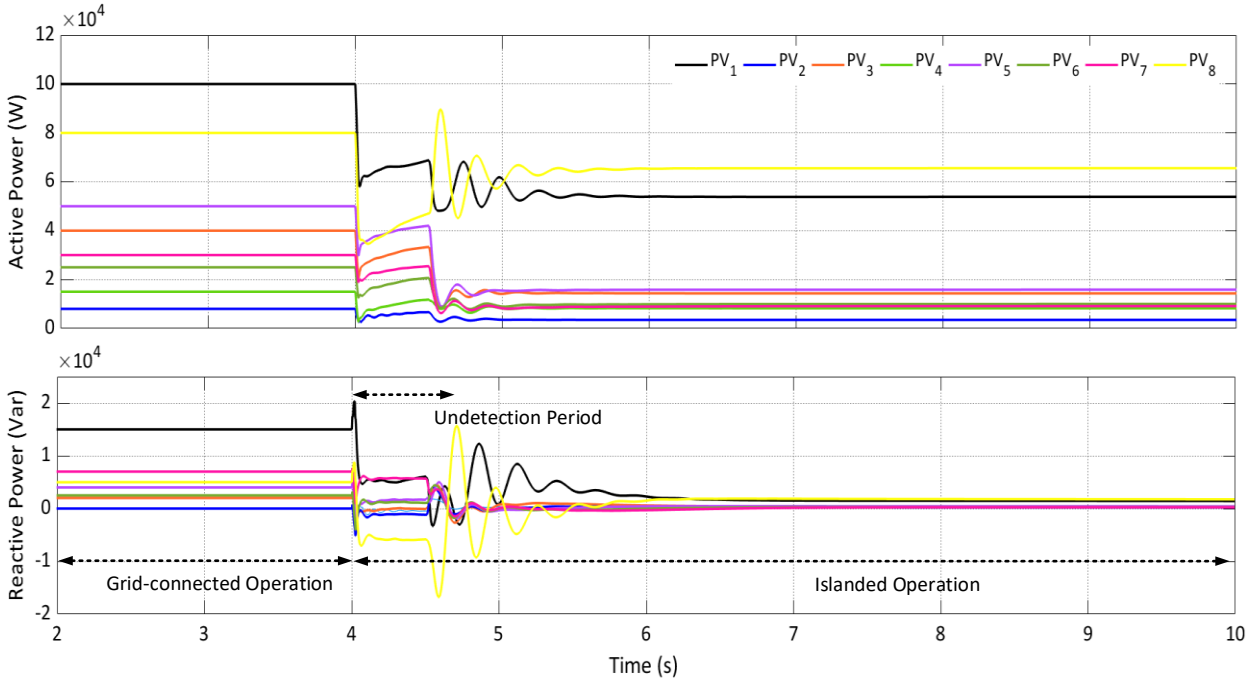

Figure 6.4: PV active and reactive power outputs in case 1.

6.1.6.3. Transition from islanded to grid-connected mode

In this scenario, the isolated grid is assumed to operate in islanded mode as a result of a fault occurred near the point of common coupling. Then, after a certain period of time, the fault is cleared, and the

isolated grid is allowed to reconnect to the distribution system. The following steps are used to verify the performance of the hierarchical controller.

- At *t = 0 – 3 (s)*, the isolated grid is operated in off-grid mode. DERs, including ES units share the load power proportional to their rate powers, governed by Power Sharing Control based on distributed consensus control.
- At t *= 3 (s)*, the isolated grid is allowed to reconnect to the distribution system, the synchronization mechanism is activated.
- At *t = 10 (s)*, the circuit breaker is closed,
- At *t = 15 (s)*, the operation mode of PVs is changed to Power Tracking Mode and their power outputs follow the setpoints from upper control level.

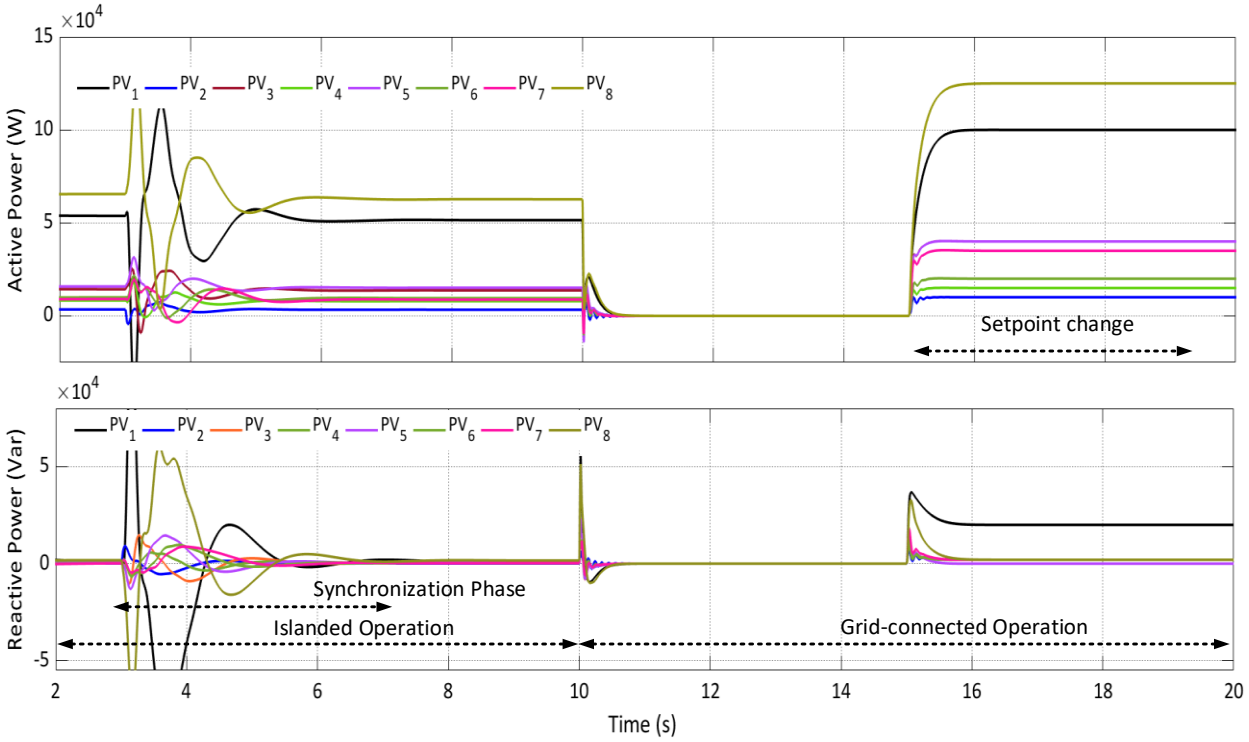

Figure 6.5: PV active and reactive power outputs in case 2.

As can be seen from Figure 6.5, as the synchronization controller sends an additional control signal to the input of the AHO, the power outputs of PV_1 change accordingly. Both active and reactive power outputs of other PVs are forced to follow the change of PV_1 in a distributed manner with different transient behaviors, as the effect of the distributed average consensus algorithm. The whole isolated grid will then converge to a new equilibrium point at which the synchronization criteria is satisfied (i.e., V_{MG} and V_{UG} are synchronized). At *t = 10 (s)*, the isolated grid is connected smoothly to the distribution system with a small transient in a short period of time. As Figure 6.5 shows, both active and reactive power-sharing among PVs is not affected by the synchronization process.

After closing the circuit breaker, the control signal S_2 is disabled, and the S_1 is activated to change the operation mode of PVs from Power Sharing Control mode to Power Tracking Control mode with the setpoints are set to 0. The active and reactive power output of PVs follows exactly the reference values.

At *t = 15 (s)*, the dispatch center calls for different step changes in P_{ref} and Q_{ref} to each PV. There is a short transient, but it vanishes quickly, and all PVs response to the setpoint changes in about 0.4 seconds.

7. Conclusions

The focus of the works presented in this report was to develop a framework for grid operation with potential risks in non-contingency and contingency operations. The works were based on the input from D3.1 as the input for system awareness to define operation risks.

The non-contingency operation with a high share of DERs can be faced with voltage rise and transformer overloading issues. Thus, in chapter 3, communities-based self-adaptive control was developed in which the customers can support the DSO in solving voltage rise and transformer overloading by adaptively changing their PV inverter control set point. By doing so, the DSO can benefit from the customer side. However, in case of the above solution cannot completely solve the voltage issue, a network reconfiguration algorithm can be used, which was developed in chapter 4. The algorithm is based on the voltage input and the current network reconfiguration to optimally select the new configuration that prevents the voltage rise issue and for loss reduction.

For the contingency operation, i.e., the system is under a stress operation with a fault or loss of elements (e.g., generator, line, or transformer). Then, an advanced model predictive control was proposed in chapter 5 to support voltage profile by coordinating load tap changers and DERs in the distribution grids. The result shows that it can quickly control the voltage after the disturbance. Furthermore, under a severe disturbance (i.e., cascading events) which can lead to system blackout, fault-initiated islanding (chapter 6) is used to disconnect a part of the grid to form an autonomous microgrid. In addition, the proposed control mechanism can re-synchronize the MG back to the main grid when the fault is cleared.

This deliverable developed a complete framework with different options for DSOs. The developed tools have been tested with the Chalmers campus network, one of the demo sites of the FlexiGrid project.

8. Appendix A: The physical data of Chalmers campus network

In this report, the Chalmers campus network is used to test our algorithms, such as adaptive control for voltage rise and transformer overloading (chapter 3), voltage rise mitigation and loss reduction (chapter 4), autonomous microgrid operation and microgrid re-synchronization (chapter 6). In addition, it is noted that the predictive model controller in chapter 5 is tested with another network due to the request of the transmission network connection.

The Chalmers network has a total electrical load demand that varies between 2.5 and 6 MW. The load demand is supplied by electricity from upstream distribution grid, and/or from a micro-combined heat and power (CHP), a battery energy storage system (BESS), and PV panels. The majority of PV panels is installed on rooftops of the campus' building with a total PV capacity is 831 kWp.

The detailed information on the Chalmers campus network can be found in the reported D5.3. The Figure 8.1 show the one-line diagram of Chalmers campus indicating highlighted renewable energy resources. The line parameter can be seen from Table 8.1.

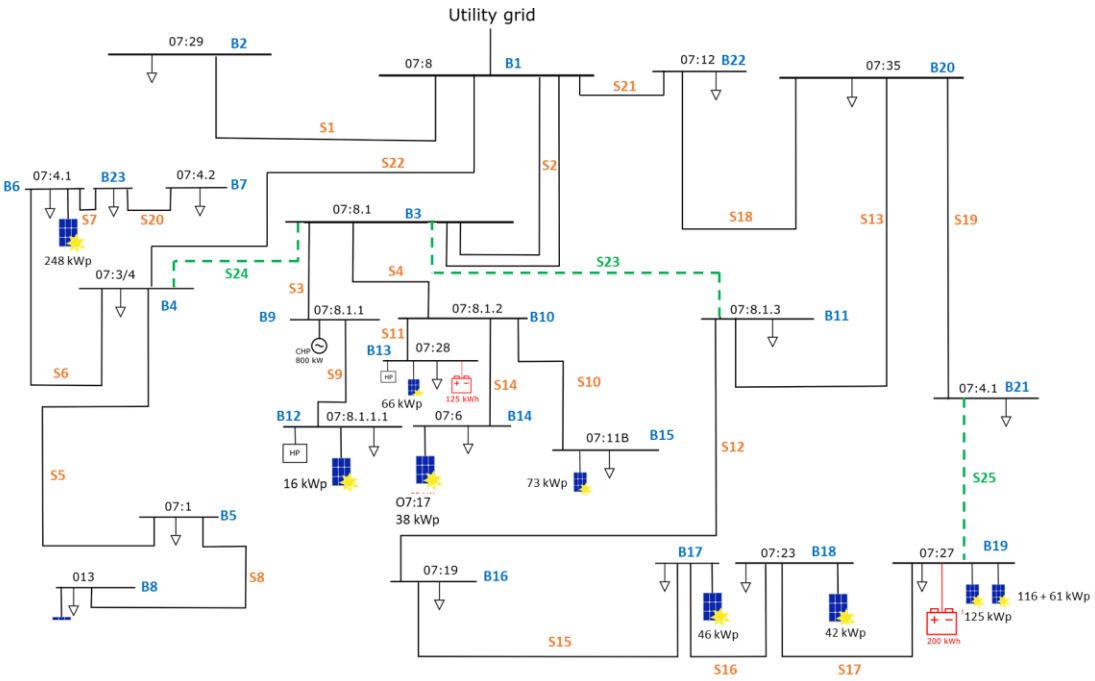

Figure 8.1: One-line diagram of Chalmers campus indicating highlighted renewable energy resources.

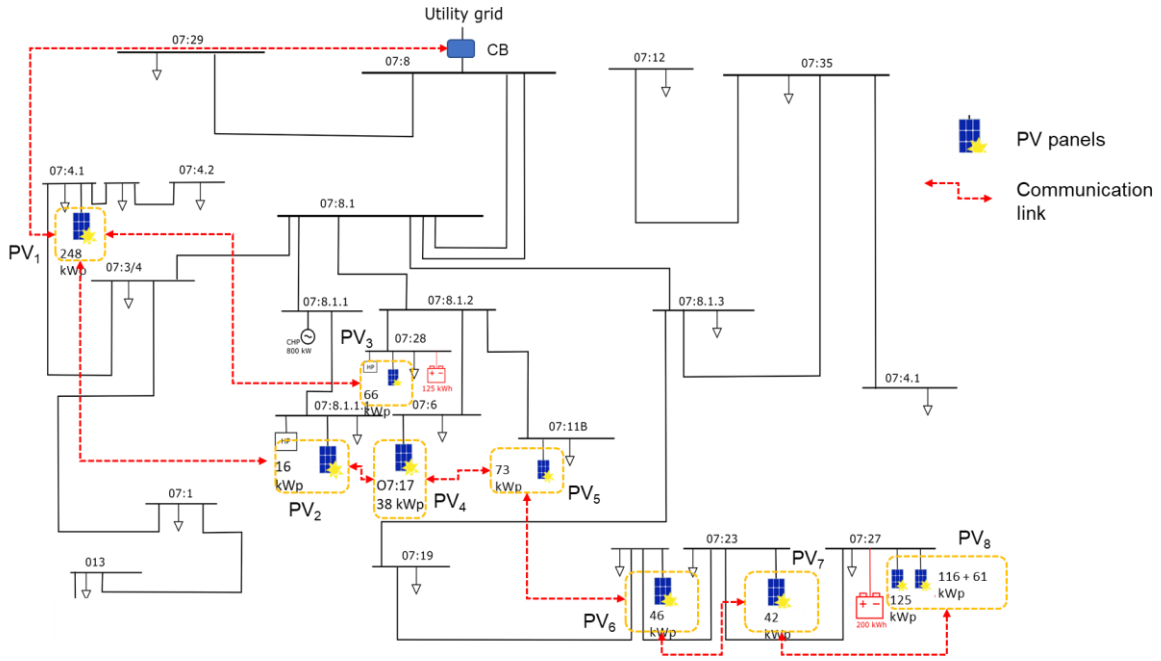

Figure 8.2: The Chalmers campus network with the communication network among PVs.

Table 8.1: Line parameter of Chalmers campus network (including some low voltage buses).

No.	From bus	To bus	R (pu)	X (pu)	B (pu)
1	1	2	1.45E-05	1.00E-06	1.70E-04
2	2	3	2.81E-05	1.90E-05	3.50E-04
3	3	4	2.55E-04	1.73E-04	3.10E-03
4	4	5	3.40E-04	2.30E-04	4.20E-03
5	5	6	1.87E-04	1.27E-04	2.30E-03
6	1	8	4.76E-04	3.23E-04	5.80E-03
7	2	10	1.72E-05	1.18E-05	2.10E-04
8	10	11	2.81E-05	1.90E-05	3.50E-04
9	2	13	2.27E-05	1.54E-05	2.80E-04
10	13	14	1.25E-04	8.44E-05	1.50E-03
11	13	16	3.75E-04	2.54E-04	4.60E-03
12	13	18	9.07E-05	6.17E-05	1.10E-03
13	2	20	3.12E-04	2.11E-04	3.80E-03
14	20	21	1.31E-04	5.80E-05	8.50E-04
15	21	22	1.87E-04	8.25E-05	1.20E-03
16	20	25	7.98E-05	5.35E-05	9.70E-04
17	25	26	8.53E-05	5.80E-05	1.00E-03
18	20	29	6.35E-05	3.08E-05	4.80E-04
19	3	31	4.54E-04	3.08E-04	5.50E-03
20	31	32	1.18E-05	8.20E-06	1.40E-04
21	32	33	3.63E-05	1.09E-05	1.20E-04
22	31	35	4.65E-04	3.16E-04	5.70E-03

9. References

[1] "EU achieves 20-20-20 climate targets, 55 % emissions cut by 2030 reachable with more efforts and policies — European Environment Agency." [Online]. Available: https://www.eea.europa.eu/highlights/eu-achieves-20-20-20. [Accessed: 02-Oct-2022].

[2] "Capaciteitskaart elektriciteitsnet." [Online]. Available: https://capaciteitskaart.netbeheernederland.nl/. [Accessed: 02-Oct-2022].

[3] J. Lindahl, "National Survey Report of PV Power Applications in Sweden 2020 Task 1 Strategic PV Analysis and Outreach PVPS."

[4] "Connecting the dots: Distribution grid investment to power the energy transition Final Deliverable," 2021.

[5] "Interim Report into the Low Frequency Demand Disconnection (LFDD) following Generator Trips and Frequency Excursion on," 2019.

[6] *UPDATE REPORT – BLACK SYSTEM EVENT IN SOUTH AUSTRALIA ON 28 SEPTEMBER 2016*. Australian Energy Market Operator, 2016.

[7] *2021 Winter Storm Uri After-Action Review: Findings Report*. City of Austin & Travis County, 2021.

[8] "RELIABILITY | RESILIENCE | SECURITY NERC | Report Title | Report Date I Multiple Solar PV Disturbances in CAISO."

[9] M. M. V. M. Ali, P. H. Nguyen, W. L. Kling, A. I. Chrysochos, T. A. Papadopoulos, and G. K. Papagiannis, "Fair power curtailment of distributed renewable energy sources to mitigate overvoltages in low-voltage networks," *2015 IEEE Eindhoven PowerTech, PowerTech 2015*, no. 608998, 2015.

[10] L. Collins and J. K. Ward, "Real and reactive power control of distributed PV inverters for overvoltage prevention and increased renewable generation hosting capacity," *Renew. Energy*, vol. 81, pp. 464–471, 2015.

[11] S. Alyami, Y. Wang, C. Wang, J. Zhao, and B. Zhao, "Adaptive real power capping method for fair overvoltage regulation of distribution networks with high penetration of PV systems," *IEEE Trans. Smart Grid*, vol. 5, no. 6, pp. 2729–2738, 2014.

[12] T. T. Mai, A. N. M. M. Haque, P. P. Vergara, P. H. Nguyen, and G. Pemen, "Adaptive coordination of sequential droop control for PV inverters to mitigate voltage rise in PV-Rich LV distribution networks," *Electr. Power Syst. Res.*, vol. 192, no. March 2020, pp. 1–13, 2021.

[13] Origami and Scottish & Southern Electricity Networks, "Analysis of relevant international experience of DSO flexibility markets," 2019.

[14] T. T. Mai, P. H. Nguyen, N. A. N. M. M. Haque, and G. A. J. M. Pemen, "Exploring regression models to enable monitoring capability of local energy communities for self-management in low-voltage distribution networks," *IET Smart Grid*, vol. 5, no. 1, pp. 1–17, 2021.

[15] K. Rahbar, C. C. Chai, and R. Zhang, "Energy cooperation optimization in microgrids with renewable energy integration," *IEEE Trans. Smart Grid*, vol. 9, no. 2, pp. 1482–1493, 2018.

[16] B. Gao, G. K. Morison, and P. Kundur, "Voltage Stability Evaluation using Modal Analysis," *IEEE*

Power Eng. Rev., vol. 12, no. 11, p. 41, 1992.

[17] ENTSO (European Network of Transmission System Operators), "General Guidelines fot Reinforcing the Cooperation Between TSOs and DSOs," *Eurelectric*, pp. 1–6, 2015.

[18] NERC (North American Electric Reliability Corp.), "Essential Reliability Services Task Force Measures Framework Report," *NERC*, no. November, pp. 1–129, 2015.

[19] H. B. Antony Zegers, "TSO-DSO interaction: An Overview of current interaction between transmission and distribution system operators and an assessment of their cooperation in Smart Grids," *ISGAN*, no. November, pp. 1–35, 2014.

[20] M. Moradzadeh, R. Boel, and L. Vandevelde, "Voltage coordination in multi-area power systems via distributed model predictive control," *IEEE Trans. Power Syst.*, vol. 28, no. 1, pp. 513–521, 2013.

[21] G. Valverde and T. Van Cutsem, "Model predictive control of voltages in active distribution networks," *IEEE Trans. Smart Grid*, vol. 4, no. 4, pp. 2152–2161, 2013.

[22] G. Prionistis, T. Souxes, and C. Vournas, "Voltage stability support offered by active distribution networks," *Electr. Power Syst. Res.*, vol. 190, no. April 2020, p. 106728, 2021.

[23] L. D. P. Ospina and T. Van Cutsem, "Power factor improvement by active distribution networks during voltage emergency situations," *Electr. Power Syst. Res.*, vol. 189, no. April, p. 106771, 2020.

[24] H. Li, F. Li, Y. Xu, D. T. Rizy, and S. Adhikari, "Autonomous and adaptive voltage control using multiple distributed energy resources," *IEEE Trans. Power Syst.*, vol. 28, no. 2, pp. 718–730, 2013.

[25] P. D. F. Ferreira, P. M. S. Carvalho, L. A. F. M. Ferreira, and M. D. Ilic, "Distributed energy resources integration challenges in low-voltage networks: Voltage control limitations and risk of cascading," *IEEE Trans. Sustain. Energy*, vol. 4, no. 1, pp. 82–88, 2013.

[26] T. T. Mai, A. N. M. M. Haque, P. P. Vergara, P. H. Nguyen, and G. Pemen, "Adaptive coordination of sequential droop control for PV inverters to mitigate voltage rise in PV-Rich LV distribution networks," *Electr. Power Syst. Res.*, vol. 192, no. July 2020, p. 106931, 2021.

[27] F. Capitanescu, I. Bilibin, and E. Romero Ramos, "A comprehensive centralized approach for voltage constraints management in active distribution grid," *IEEE Trans. Power Syst.*, vol. 29, no. 2, pp. 933–942, 2014.

[28] H. M. Nguyen, J. L. R. Torres, A. Leki, and H. V. Pham, "MPC Based Centralized Voltage and Reactive Power Control for Active Distribution Networks," *IEEE Trans. Energy Convers.*, vol. 36, no. 2, pp. 1537–1547, 2021.

[29] H. Cai, H. Ma, and D. J. Hill, "A Data-Based Learning and Control Method for Long-Term Voltage Stability," *IEEE Trans. Power Syst.*, vol. 35, no. 4, pp. 3203–3212, 2020.

[30] M. Q. Tran, T. T. Tran, P. H. Nguyen, and L. A. Tuan, "Coordination of Load Tap Changer and Distributed Energy Resources to Improve Long-term Voltage Stability Coordination of Load Tap Changer and Distributed Energy Resources to Improve Long-term Voltage Stability," *EnergyCon 2022 Inst. Electr. Electron. Eng.*, 2022.

[31] Y. Han, P. Shen, X. Zhao, and J. M. Guerrero, "Control Strategies for Islanded Microgrid Using Enhanced Hierarchical Control Structure with Multiple Current-Loop Damping Schemes," *IEEE Trans. Smart Grid*, vol. 8, no. 3, pp. 1139–1153, 2017.

[32] Q. C. Zhong, P. L. Nguyen, Z. Ma, and W. Sheng, "Self-synchronized synchronverters: Inverters without a dedicated synchronization unit," *IEEE Trans. Power Electron.*, vol. 29, no. 2, pp. 617–630, 2014.

[33] I. Sowa, T. T. Tran, T. Heins, D. Raisz, and A. Monti, "An Average Consensus Algorithm for Seamless Synchronization of Andronov-Hopf Oscillator Based Multi-Bus Microgrids," *IEEE Access*, vol. 9, pp. 90441–90454, 2021.

[34] T. T. Tran, I. Sowa, D. Raisz, and A. Monti, "An average consensus-based power-sharing among VOC-based distributed generations in multi-bus islanded microgrids," *IET Gener. Transm. Distrib.*, vol. 15, no. 4, pp. 792–807, 2021.

[35] M. H. Roos, M. F. Faizan, P. H. Nguyen, J. Morren, and J. G. Slootweg, "Probabilistic Adequacy and Transient Stability Analysis for Planning of Fault-initiated Islanding Distribution Networks," in *2021 IEEE Madrid PowerTech, PowerTech 2021 - Conference Proceedings*, 2021.

[36] H. Laaksonen, "Advanced islanding detection functionality for future electricity distribution networks," *IEEE Trans. Power Deliv.*, vol. 28, no. 4, pp. 2056–2064, 2013.

[37] D. Houseman, "APPLYING MODERN COMMUNICATION TECHNOLOGY TO LOSS-OF-MAINS PROTECTION," no. 0012, pp. 8–11, 2009.

[38] F. Coffele *et al.*, "Centralised loss of mains protection using IEC-61850," *IET Conf. Publ.*, vol. 2010, no. 558 CP, pp. 1–5, 2010.

[39] K. N. E. Ku Ahmad, J. Selvaraj, and N. A. Rahim, "A review of the islanding detection methods in grid-connected PV inverters," *Renew. Sustain. Energy Rev.*, vol. 21, pp. 756–766, 2013.

[40] A. Khamis, H. Shareef, E. Bizkevelci, and T. Khatib, "A review of islanding detection techniques for renewable distributed generation systems," *Renew. Sustain. Energy Rev.*, vol. 28, pp. 483–493, 2013.

[41] B. Kumar Panigrahi, R. Nandi, B. Mahanta, and K. Pal, "Islanding detection in distributed generation," *Proc. IEEE Int. Conf. Circuit, Power Comput. Technol. ICCPCT 2016*, pp. 0–4, 2016.

[42] C. F. Ten and P. A. Crossley, "Evaluation of ROCOF relay performances on networks with distributed generation," *IET Conf. Publ.*, no. 536 CP, pp. 522–527, 2008.

[43] V. Menon and M. H. Nehrir, "A hybrid islanding detection technique using voltage unbalance and frequency set point," *IEEE Trans. Power Syst.*, vol. 22, no. 1, pp. 442–448, 2007.

[44] M. Lu, S. Dutta, V. Purba, S. Dhople, and B. Johnson, "A grid-compatible virtual oscillator controller: Analysis and design," *2019 IEEE Energy Convers. Congr. Expo. ECCE 2019*, pp. 2643–2649, 2019.